Escola d'Enginyeria de Telecomunicació i Aeroespacial de Castelldefels
UNIVERSITAT POLITÈCNICA DE CATALUNYA

TREBALL FINAL DE GRAU

TFG TITLE: Hysteretical behaviour of a NACA 0012 airfoil at ultralow Reynolds upon variation of the angle of attack.

DEGREE: Grau en Enginyeria d'Aeronavegació

AUTHOR: Jordi Bergillo Cortés

ADVISOR: Fernando Mellibovsky Elstein

DATE: September 24th, 2017

Títol: Comportament d'histèresi d'un perfil NACA 0012 per Reynolds ultra baixos sobre variació de l'angle d'atac.

Autor: Jordi Bergillo Cortés

Director: Fernando Mellibovsky Elstein

Data: 24 de setembre del 2017

Resum

Els estudis a baixos nombres de Reynolds son necessaris per entendre la física que envolta l'aerodinàmica a nombres de Reynolds més grans on els fenòmens que apareixen son cada vegada més complexos i es molt necessari utilitzar models matemàtics per tal de modelar el que passa. El nostre escenari està descrit per un Reynolds de 5300 i per aquesta configuració trobem un cas d'histèresis aerodinàmica al voltant dels 7º d'angle d'atac. Trobem la coexistència de dos solucions per aquests valors i volem demostrar que hi ha una tercera solució inestable que connecta les altres dues. Per poder fer això tindrem que utilitzar la dinàmica de fluids computacional per tal de trobar solució a les equacions de Navier-Stokes que governen el nostre cas i poder fer les simulacions adients. El mètode que utilitzarem per determinar la existència d'aquesta solució inestable és el Edge Tracking. Aquest mètode ens permetrà determinar quines son les condicions inicials necessàries per tal de caure a la solució inestable. Quanta més precisió anem aconseguint amb cada iteració, més temps aconseguirem estar a sobre de la frontera de la regió inestable abans que sigui atret per una de les estables. A més, estudiarem les distintes solucions obtingudes i les comparem amb d'altres per tal de fer una bona descripció. Compararem les forces aerodinàmiques, però també dos fenòmens com son el despreniment de capa límit o el *vortex shedding,* fent per aquest últim un anàlisi en freqüència mitjançant la transformada de Fourier. Finalment, hem aconseguit demostrar la existència de la regió inestable per el nostre escenari d'estudi.

Title: Hysteretical behaviour of a NACA 0012 airfoil at ultralow Reynolds upon variation of the angle of attack.

Author: Jordi Bergillo Cortés

Director: Fernando Mellibovsky Elstein

Date: September 24th 2017

Overview

Reynolds's low numbers studies are necessary to understand the physics surrounding aerodynamics in larger Reynolds numbers where the phenomena they appear are becoming increasingly complex and it is very necessary to use mathematical models to model what is happening. Our scenario is described by a Reynolds of 5300 and for this configuration we find a case of aerodynamic hysteresis around the 7º angle of attack. We find the coexistence of two solutions for these values and we want to show that there is a third unstable solution that connects the other two. In order to do this, we will have to use computational fluid dynamics in order to find a solution to the Navier-Stokes equations that govern our case and to be able to do the appropriate simulations. The method that we will use to determine the existence of this unstable solution is Edge Tracking. This method will allow us to determine what are the initial conditions necessary to fall to the unstable solution. The more accurate we are achieving with each iteration, the more time we will be able to be above the boundary of the unstable region before it is attracted to one of the stables. In addition, we will study the different solutions obtained and compare them with others in order to make a good description. We will compare the aerodynamic forces, but also two phenomena such as the detachment of the boundary layer or the vortex shedding, making the latter a frequency analysis using the Fourier transform. Finally, we have succeeded in demonstrating the existence of the unstable region for our study scenario.

INDEX

LIST OF FIGURES

LIST OF TABLES

INTRODUCTION

Low-Reynolds studies are important to can understand the physics basics of aerodynamics and can extrapolate some cases to high-Reynolds studies where things get complex. But this is not the only we have to consider. We are living the growth of the UAV sector, where low-Reynolds numbers govern a huge part of this sector.

Our particular study is going to focus in a detailed phenomenon which occurs at AoA 7º and number of Reynolds equals to 5300. This phenomenon is called hysteresis and refers to a coexistence of two solutions [1]. Hysteresis occurs not only occurs for our selected angle of attack, it exists also for other values. But we are only try to describe the one which occurred at AoA 7º. We try to demonstrate that there is a connection between these two solutions that is a third solution. This third solution is unstable. Other solutions at different angles of attack will help us comparing the different performances obtained.

The equations that governs this aerodynamic problem are the Navier-Stokes equations. These equations only have analytical solution for very simple geometries, but there is not our case. Therefore, numerical methods are required for the resolution of these differential equations. We use the software Nektar++ to can achieve these simulations and can get results. With this tool of computational fluid dynamics, we are going to solve the Navier-Stokes equation for different scenarios we are going to create.

As the time that simulations require is quite high, we will need to make some modifications on the mesh, performed with the software Gmsh, to can reduce this time. We cannot forget that we are committing error when doing that so we have to compute the error and try to do not pass an error threshold. We also try to reduce more resolution on parts of the mesh that are not as important as the wake or near the airfoil. With the help of the software Octave we can compute the error committed by reducing the mesh resolution.

The method required to characterize the unstable solution is the edge tracking method, a kind of bisection that will lead us to get accurate and put us as near as possible of the unstable solution to be as much time as possible on it to describe it [2]. By getting more accurate, this solution will be longer in time and we will be able to study it.

As Nektar++ is just a solver, some extra software as Paraview and Xmgrace will help us to postprocess all the information we get and let us to make a good analysis of the different solutions that exists at AoA 7º. Paraview is the tool in charge of drawing the velocity field, vorticity field… Meanwhile Xmgrace has been useful to plot the aerodynamic forces and to make Fourier transforms for frequency analysis.

There are some phenomena that we consider significant to compare. These are the boundary layer detachment and the vortex shedding. To do not limit the study

to only the aerodynamic forces, we also help the description of the different solutions by characterizing these phenomena. We will see the impact each phenomenon has on angle of attack or the relation with lift or drag.

CHAPTER 1. THEORETICAL FRAMEWORK

1.1. Reynolds number

It is known for everybody the important growth on the UAV sector. There are huge ones as Predator models and by other hand the not as big at all. There are several models which their dimensions are quite small, parameters as chord, velocity, flight altitude… In fact, low Reynolds number. Low-Reynolds number aerodynamics has become increasingly important of late due to interest in the development of unmanned aerial vehicles. The Reynolds number is an dimensionless parameter that comes out between the relation of the inertial and viscous forces in the Navier-Stokes equations which later will be discussed in section 1.2.

$$Re = \frac{V \cdot c}{\nu} \quad \textbf{(1.1)}$$

where V is the fluid velocity, c is the airfoil chord and *v* the kinematic viscosity.

In an experimental way, it is observed that for low Reynolds numbers the fluid movement is laminar and prevail the friction forces; while for higher Reynolds number the fluid movement is turbulent and predominate the inertial forces.

In our study, we are working with Re=5300, is a low value compared with commercial aircraft, but not big enough to get in the turbulent range.

1.2. Navier-Stokes equations

The scenario we want to simulate is governed by the Navier-Stokes equations which describe the motion of viscous fluid substances. Being more accurate, we need the incompressible Navier Stokes in 2D for viscous Newtonians fluids governed by:

$$\frac{\partial V}{\partial t} + V \cdot \nabla V = -\nabla p + \nu \nabla^2 V + f \quad \textbf{(1.2)}$$

$$\nabla \cdot V = 0 \quad \textbf{(1.3)}$$

where V is the velocity, p is the specific pressure (including density) and *v* the kinematic viscosity.

As we previously know, there is no analytical solution for resolving the equations. Therefore, numerical methods are needed. We used the software Nektar++, a spectral/hp element framework, where we can use the proper solver. In similar way as other simulation software, the basis of the calculations is to divide the surface or volume in a useful form by cells or blocks, depends the dimensions of the problem. Then, numeric methods are used to filling the cells with values, and

then iterate several times until the solution converges into a value. Getting more focus on Nektar++, the method we used in our simulations is known as Velocity Correction Scheme, which is commonly used in the numerical solution of unsteady incompressible flows. The velocity-correction scheme is a time-integration method for the unsteady incompressible Navier–Stokes equations and this method has the advantage of allowing the pressure and the velocity to be solved separately, leading to an efficient solution.

Another fact involved with the characteristics of our simulation method, is the continuous Galerkin approach. On this approach, continuity of the expanded variables is imposed across the element boundaries of the mesh. To get more information of the Navier-Stokes resolution get to the Nektar++ user's manual [3].

1.3. Airfoil and mesh

In this aerodynamical study, the most important piece and object of study is the airfoil. The selected one is de NACA 0012. The word NACA is an acronym of National Advisory Committee for Aeronautics and its airfoils are airfoils shapes for aircraft wings. Its shape is described by the digits following the NACA. In our case we have a four-digit airfoil. The first pair of digits tells us information about the camber. As we have a pair of zeros, it implies there is no camber, so the airfoil is symmetrical. By other hand, we have the right-handed pair of digits on where we have a twelve. This pair of digits brings us information about the thickness to chord length ratio. So, this NACA 0012 is a symmetrical with 12% as thick as it is long. We have chosen this airfoil because is a standard form and one of the simplest airfoils. We think is a good election for the object of our study because of the simplicity of its shape and also this airfoil is a benchmark of aerodynamical studies. On Figure 1.1 is showed a representation in two and three dimensions of the NACA 0012.

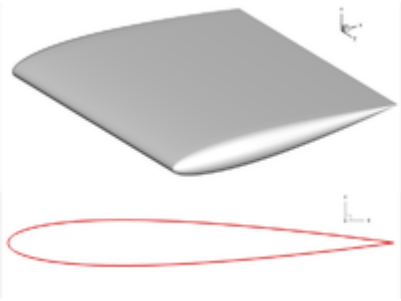

Figure 1.1: NACA 0012, 2D and 3D representation.

Once the airfoil has been selected yet, it has to be modelized in order that the software Nektar++ can work with it. The first pass is modelling the geometry. To achieve that we use Gmsh [4], a three-dimensional finite element mesh generator with built-in pre- and post-processing facilities.

The following step is to create an appropriate mesh. Recall that because the fact of the no existence of analytical solution to the Navier-Stokes, the discretization of the surface or volume is needed to solve them. That is the aim of the creation of a mesh. As we will need changes in the angle of attack we need an optimized parametrical mesh, or what is the same, that changes in parameters can be done without breaking the cohesion of the mesh.

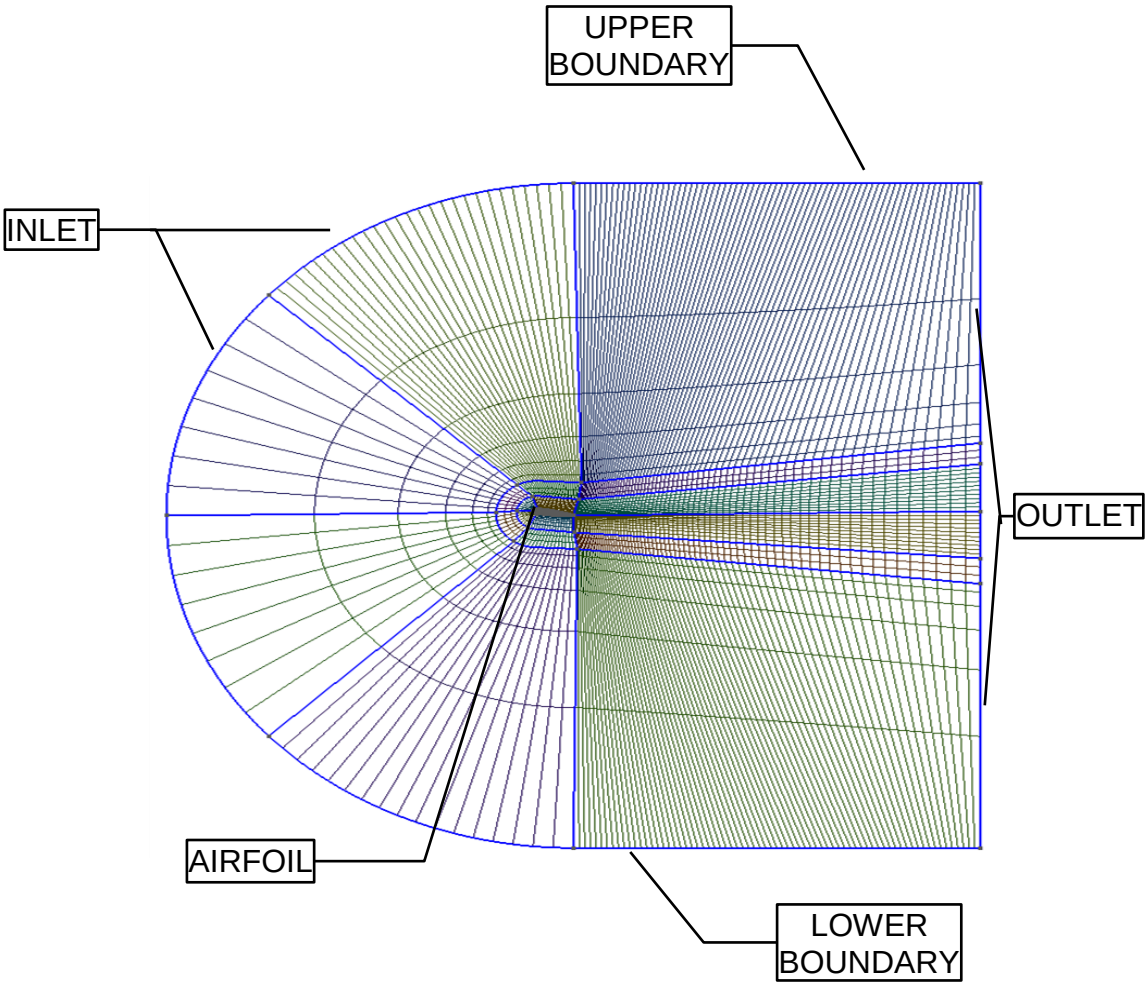

Figure 1.2: Full resolution mesh

In the Figure 1.2 we show an example of the mesh including the airfoil for an AoA (Angle of Attack) of 9º. This configuration is the full resolution one, there is enough cells to do not lose information. There are zones with wider cells and other parts where the cells are so small in order to be more accurate on critic areas where there is important information such as near the airfoil and the wake. Figure 1.3 is a zoom from the previous one where it can be seen in more detail the importance of regions just concerning in the extension of the surface of cells.

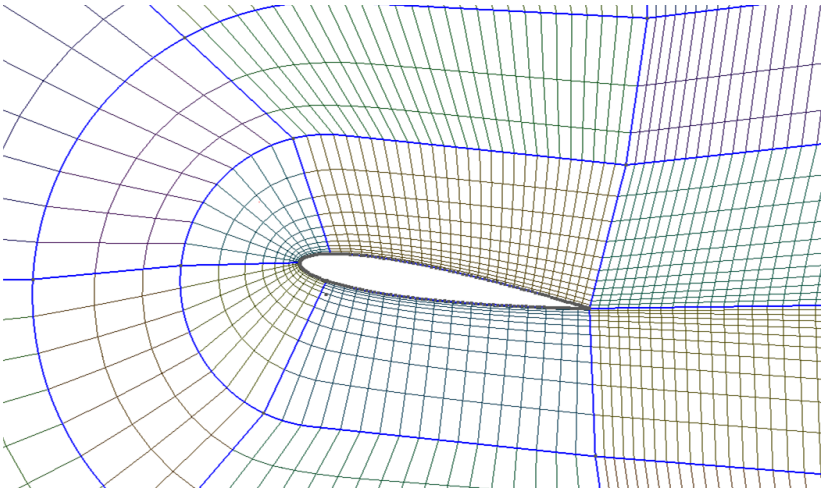

Figure 1.3: Zoom from the mesh near airfoil.

Notice that all the mesh is composed by quadrilateral elements. That is why because we decided to implant a structured mesh. Gmsh includes an algorithm which simplifies a lot when making a structured mesh, the Transfinite algorithm. Just exposing the number of points a line will be partitioned and the progression between them.

By other hand, we are going to get more focused on describing what this simulation is made of. Once we have selected our desired airfoil, it is time to get in it into simulation space. The software configures it as in real life there are wind tunnels. As shown before, the mesh is delimited by some edges which are the walls of the surface control.

Also in Figure 1.2 it is labelled the different parts that conform the control surface where Navier-Stoker equations will be solved within. First, starting by left, we have the inlet. The inlet is the only boundary on which fluid enter is configured. On Section 1.4 more details on how it is set. Then we have the boundaries, both upper and lower, that just delimits the surface. They are far enough to do not disturb solution making tunnel effect and do not lose information. Finally, we have the outlet, just the opposed to the inlet, where the fluid exits.

There is another division of surfaces inside the control surface. It is not as general as the described before and its utility will be seen on next section when referring to the polynomial expansions used within the elements. This division let us to treat in a different way each surface by its importance to us in an easy way. We remarked this surfaces with colour to make easier its distinction in Figure 1.4:

- Black: farfield.
- Red: midfield
- Yellow: upper nearfield
- Cyan: lower nearfield
- Green: wake
- Grey: upper wake

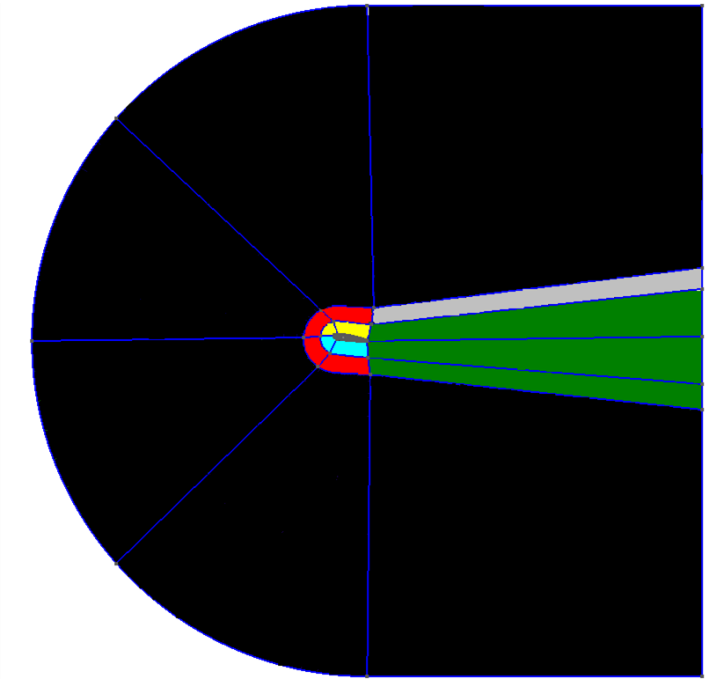

Figure 1.4: Mesh surfaces

1.4. XML files

One particularity of Nektar++ is the absence of graphic interface. The form of operation is simply: you enter some inputs; the program works on it and finally gives you some outputs. Figure 1.5 is a diagram of how Nektar++ works. All is done by the console; the operative system used is Ubuntu. The language our solver understands is XML format.

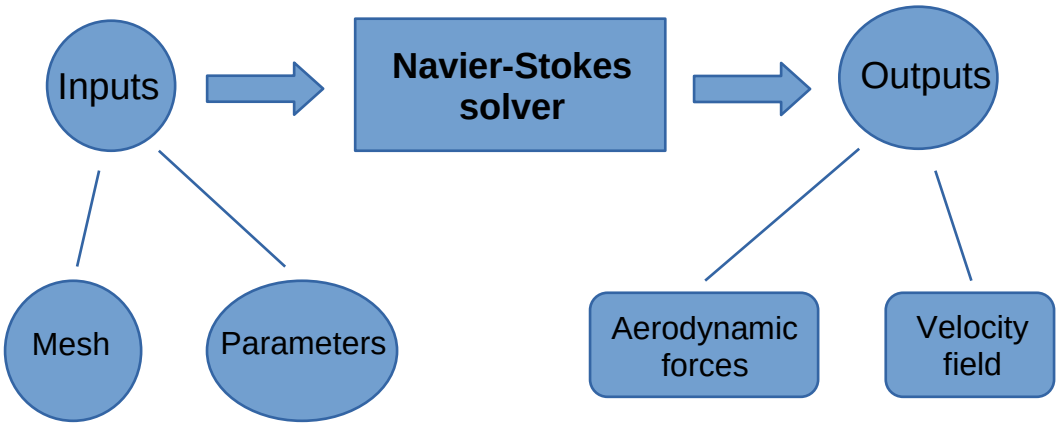

Figure 1.5: Diagram of Nektar++

There are several solvers and tools included in Nektar++, but the one which we will use to solve the Navier-Stokes equations is the *IncNavierStokesSolver*. The syntax when calling the solver at the console is adding an XML file that will be the input. This input includes information about the mesh and the parameters or

conditions of the simulation. For easy and better organization with files, we decided to divide into two different files the input. One file for the mesh and the other one for the parameters of the simulation. The outputs we obtain are also without graphic interface, therefore it will be files that are created. So, it implies the utilization of more software for post-processing data. The output files we want to create depends on our choice, in the xml file of parameters you can choose which type of outputs you need.

1.4.1 Mesh

The first file includes all the information about the geometry codified in xml format. As previously mentioned, we used the software Gmsh for the meshing mission. The format this program works with is a *.msh* extension. Nektar++ includes a tool *NekMesh* which makes possible to change the format of a mesh turning it into a xml file in just one console line.

Figure 1.6: Mesh XML file.

All the file is in xml format and some parts are codified, but we can distinguish the different parts that conform the mesh. In Figure 1.6 is showed the vertex part that includes all the points which conforms a quadrilateral element.

Figure 1.7: Edge part from mesh.xml file.

The vertex part is followed by the conjunction of two vertex, the edge. An edge is the line created when associating two vertices. In Figure 1.7 we appreciate this part is also codified. Same as it occurs between vertex and edges, an “element” is a surface formed by edges. Notice that in our particular case, all of our elements will be formed by groups of four edges.

```
        <COMPOSITE>
            <C ID="1"> E[318,321,323-324,612,614,616,618,270,273,275,277,279,281
,283,285,287,289,291,293,295-296,575,577,579,581,583,585,587,589,591,593] </C>
            <C ID="2"> E[1233,1290,1347,1404,1461,1518,1548,702,759,789,83,140,1
97,1857,1914,1971,2028,2085,2142,2171,981,1039,1068,408,466,523] </C>
            <C ID="3"> E[1589,1586,1583,1580,1577,1574,1571,1568,1565,1562,1559,
1556,1553,1549,1755,1752,1749,1745] </C>
            <C ID="4"> E[2201,2199,2196,2193,2190,2187,2184,2181,2178,2175,2322,
2320,2317,2314] </C>
            <C ID="5"> E[143,146,148,150,152,154,156,158,160,162,164,166,168,170
,172,174,176,178,180,182,184,186,188,190,192,194,196,198] </C>
            <C ID="6"> E[468,470,472,474,476,478,480,482,484,486,488,490,492,494
,496,498,500,502,504,506,508,510,512,514,516,518,520,522] </C>
            <C ID="7"> Q[0-263] </C>
            <C ID="8"> Q[264-347] </C>
            <C ID="9"> Q[348-527] </C>
            <C ID="10"> Q[724-849] </C>
            <C ID="11"> Q[1046-1143] </C>
            <C ID="12"> Q[528-723,850-1045] </C>
        </COMPOSITE>
        <DOMAIN> C[7,8,9,10,11,12] </DOMAIN>
```

Figure 1.8: Composite and domain parts from mesh.xml file.

Finally, we create the composites, that are conformed by groups of edges and other ones by group of elements. The first six composites, which are an association of edges, are the physical lines that delimits the control surface. By other hand, the last six composites are all elements, or physical surfaces, which are contained inside the control surface. Finally, the domain is the group of composites where the simulation is going to be considered as a fluid and can be discretized and resolved the Navier-Stokes equations. In Figure 1.8 it can be observed in a clearer way.

1.4.2 Parameters

The other file, but not least important, is the file where it is contained the information and settings of the simulation. With any text editor such as EMACS it is possible to change values and conditions in this file.

```
<?xml version="1.0" encoding="utf-8" ?>
<NEKTAR>

  <EXPANSIONS>
    <E COMPOSITE="C[7]" NUMMODES="4" TYPE="MODIFIED" FIELDS="u,v,p" /> <!-- FarField -->
    <E COMPOSITE="C[8]" NUMMODES="6" TYPE="MODIFIED" FIELDS="u,v,p" /> <!-- UpperMidFieldWake -->
    <E COMPOSITE="C[9]" NUMMODES="6" TYPE="MODIFIED" FIELDS="u,v,p" /> <!-- MidFieldExceptUpperWake -->
    <E COMPOSITE="C[10]" NUMMODES="8" TYPE="MODIFIED" FIELDS="u,v,p" />  <!-- UpperNearField -->
    <E COMPOSITE="C[11]" NUMMODES="8" TYPE="MODIFIED" FIELDS="u,v,p" />  <!-- LowerNearField -->
    <E COMPOSITE="C[12]" NUMMODES="8" TYPE="MODIFIED" FIELDS="u,v,p" />  <!-- Wake -->
  </EXPANSIONS>
```

Figure 1.9: Expansions section in parameters file.

First, we find is the expansions definition. This section defines the polynomial expansions used on each of the defined geometric composites. That is why there is a difference between some of the expansions modes. The nearer is the physical area from the airfoil, the higher order must be. The most critical parts are the wake and the surfaces in contact with the airfoil, zones where more useful

information we will collect. In section field, we are able to specify the calculation fields we desired. We are interested in calculate the velocity field, as we are in a 2D model, only the *u* and *v* components. It is also important to compute the pression field. In Figure 1.9 is showed the format as it appears in the text editor.

```
<CONDITIONS>
  <SOLVERINFO>
    <I PROPERTY="SOLVERTYPE"              VALUE="VelocityCorrectionScheme"        />
    <I PROPERTY="EQTYPE"                  VALUE="UnsteadyNavierStokes"    />
    <I PROPERTY="Projection"              VALUE="Continuous"              />
    <I PROPERTY="EvolutionOperator"       VALUE="Nonlinear"               />
    <I PROPERTY="TimeIntegrationMethod"   VALUE="IMEXOrder2"              />
    <I PROPERTY="Driver"                  VALUE="Standard"                />
    <I PROPERTY="AdvectionForm"           VALUE="SkewSymmetric"           />
    <I PROPERTY="Extrapolation"           VALUE="Standard"                />
  </SOLVERINFO>
```

Figure 1.10: Simulation conditions in parameters file.

The next section in Figure 1.10 describes the characteristics of the simulation. These properties have been discussed yet at Section 1.2, when Navier-Stokes equation and how Nektar++ software works on them.

```
<PARAMETERS>
  <P> TimeStep      = 0.0002    </P>
  <P> NumSteps      = 1000000   </P>
  <P> IO_CheckSteps = 50000     </P>
  <P> IO_InfoSteps  = 100       </P>
  <P> Re            = 5300      </P>
  <P> Kinvis        = 1./Re     </P>
  <P> aoa           = 09        </P>
  <P> OutflowBC_theta  = 1.0    </P>
  <P> OutflowBC_alpha1 = 1.0    </P>
  <P> OutflowBC_alpha2 = 0.0    </P>
  <P> D0            = 1.0       </P>
  <P> Kinvis        = 1./Re     </P>
</PARAMETERS>

<VARIABLES>
  <V ID="0"> u </V>
  <V ID="1"> v </V>
  <V ID="2"> p </V>
</VARIABLES>

<BOUNDARYREGIONS>
  <B ID="0"> C[1] </B> <!-- Inlet -->
  <B ID="1"> C[2] </B> <!-- Outlet -->
  <B ID="2"> C[3] </B> <!-- Upper Surface -->
  <B ID="3"> C[4] </B> <!-- Lower Surface -->
  <B ID="4"> C[5] </B> <!-- Upper Boundary -->
  <B ID="5"> C[6] </B> <!-- Lower Boundary -->
</BOUNDARYREGIONS>
```

Figure 1.11: Parameters and boundary region in parameters file.

On Figure 1.11, more parameters of simulation are defined, such as the time corresponding to each step, the number of steps, the Reynolds number… And also, the variables are declared, velocity and pression. Same as occurred with expansions, the boundary regions need to be defined in same way with the

composites that were composed by edges, they were the inlet, outlet… described in Section 1.3.

```
<BOUNDARYCONDITIONS>
  <REGION REF="0">
    <D VAR="u" VALUE="1" />
    <D VAR="v" VALUE="0" />
    <N VAR="p" USERDEFINEDTYPE="H" VALUE="0"/>
  </REGION>
  <REGION REF="1">
    <R VAR="u" USERDEFINEDTYPE="HOutflow" VALUE="0" PRIMCOEFF="D0/TimeStep" />
    <R VAR="v" USERDEFINEDTYPE="HOutflow" VALUE="0" PRIMCOEFF="D0/TimeStep" />
    <R VAR="p" USERDEFINEDTYPE="HOutflow" VALUE="0" PRIMCOEFF="1.0/(D0*Kinvis)" />
  </REGION>
  <REGION REF="2">
    <D VAR="u" VALUE="0" />
    <D VAR="v" VALUE="0" />
    <N VAR="p" USERDEFINEDTYPE="H" VALUE="0" />
  </REGION>
  <REGION REF="3">
    <D VAR="u" VALUE="0" />
    <D VAR="v" VALUE="0" />
    <N VAR="p" USERDEFINEDTYPE="H" VALUE="0" />
  </REGION>
  <REGION REF="4">
    <N VAR="u" VALUE="0" />
    <D VAR="v" VALUE="0" />
    <N VAR="p" USERDEFINEDTYPE="H" VALUE="0" />
  </REGION>
  <REGION REF="5">
    <N VAR="u" VALUE="0" />
    <D VAR="v" VALUE="0" />
    <N VAR="p" USERDEFINEDTYPE="H" VALUE="0" />
  </REGION>
</BOUNDARYCONDITIONS>
```

Figure 1.12: Boundary conditions section on parameters file.

On Figure 1.12 there is the setup of the boundaries. The inlet (region 0) is the only boundary from which the flux enters the control surface. The velocity inlet is set unitary on its horizontal component, meanwhile vertical component and also normal pressure gradient is taken as zero. On region 1, the outlet, we set the pressure and the normal gradient for velocity component to zero and it can evolve with simulation. Regions 2 and 3 corresponds to the airfoil and there is non-slip wall condition, zero velocity and high order pressure gradient. Finally, regions 4 and 5 are the upper and lower boundaries. Here there is imposed the condition of slip-walls by setting velocity to zero and the normal *u* and pression gradients too.

```
  <FUNCTION NAME="InitialConditions">
    <E VAR="u" VALUE="0" />
    <E VAR="v" VALUE="0" />
    <E VAR="p" VALUE="0" />
  </FUNCTION>

</CONDITIONS>
```

Figure 1.13: Function section on parameters file.

Last part on conditions section corresponds to the function part. Multi-variable functions such as initial conditions and analytic solutions may be specified for use in simulations, as shown in Figure 1.13. This part will become an important part

because we will be able to change initial conditions. Making these changes and other one that later will be exposed it could be possible to find the hysteresis zone. Initial conditions we set them up from null conditions or by reading them from a previous simulation file.

```
  <FILTERS>
    <FILTER TYPE="HistoryPoints">
      <PARAM NAME="OutputFile">naca0012A09Re5300.h25.1</PARAM>
      <PARAM NAME="OutputFrequency">10</PARAM>
      <PARAM NAME="Points">
        -9.9 0.0 0.0
        1.9131 0.20791 0.0
        2.9131 0.20791 0.0
        3.9131 0.20791 0.0
      </PARAM>
    </FILTER>
    <FILTER TYPE="AeroForces">
      <PARAM NAME="OutputFile">naca0012A09Re5300.h25.1</PARAM>
      <PARAM NAME="StartTime">0</PARAM>
      <PARAM NAME="OutputFrequency">10</PARAM>
      <PARAM NAME="Boundary">B[2,3]</PARAM>
      <PARAM NAME="Direction1">
        1 0 0
      </PARAM>
      <PARAM NAME="Direction2">
        0 1 0
      </PARAM>
    </FILTER>
  </FILTERS>

</NEKTAR>
```

Figure 1.14: Filters section in parameters file.

We previously talk about the outputs Nektar++ creates, these are the filters. Filters are a method for calculating a variety of useful quantities from the field variables as the solution evolves in time, such as aerodynamic forces and extracting the field variables at certain points inside the domain. We have decided that it will be useful the extraction of history points. The history points filter can be used to evaluate the value of the fields in specific points of the domain as the solution evolves in time. For each timestep, and then each history point, a line is output containing the current solution time, followed by the value of each of the field variables. Another crucial output we need to extract are the aerodynamic forces. This filter evaluates the aerodynamic forces along a specific surface. The forces are projected along the Cartesian axes and the pressure and viscous contributions are computed in each direction. We specify the file we want to create with them and the axes were the forces will be projected. Finally, the last filter we used, in that case also as a safety election. The checkpoint filter writes a checkpoint file, containing the instantaneous state of the solution fields at given timestep. This can subsequently be used for restarting the simulation or examining time-dependent behaviour. We show on Figure 1.14 all the selected filters.

1.5. Hysteresis and edge tracking method

It is well known the importance of studies at low-Reynolds number. At this region, it occurs several phenomena that help us to understand the aerodynamics at higher Reynolds number. One of these phenomena, and an aim of this project, is the hysteresis. Hysteresis is a widely occurring phenomenon. It can be found in a large variety of natural and constructed systems. In our particular case, we define this hysteresis as the coexistence of two solutions for a same AoA. It depends on the initial conditions if we will finally end on one or another solution. Therefore, aerodynamical characteristics for an airfoil could change having a strong dependence on its history. Qualitatively, in Figure 1.15 we try to represent this phenomenon applied to our particular case for help visualization.

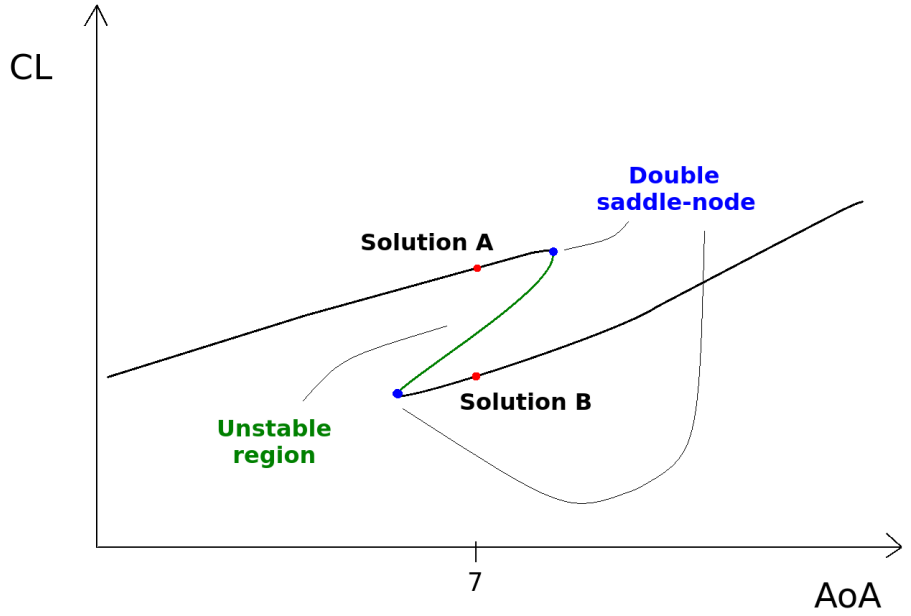

Figure 1.15: Hysteresis case at AoA 7º.

If we take a look at the figure above, we can distinguish a double saddle node. We arrive to both different solutions obtainment at AoA 7º. First solution A, is achieved by just simulating with null initial conditions. Solution B differs from A in that we have changed initial conditions, starting now from an AoA of 8º. If we continue from A increasing the angle of attack we will fall down to the straight line that governs B. Same it will occurs if we start from B and start decreasing the angle of attack, we will jump to the upper region. This hysteresis loop is described in Figure 1.16 with remarked line.

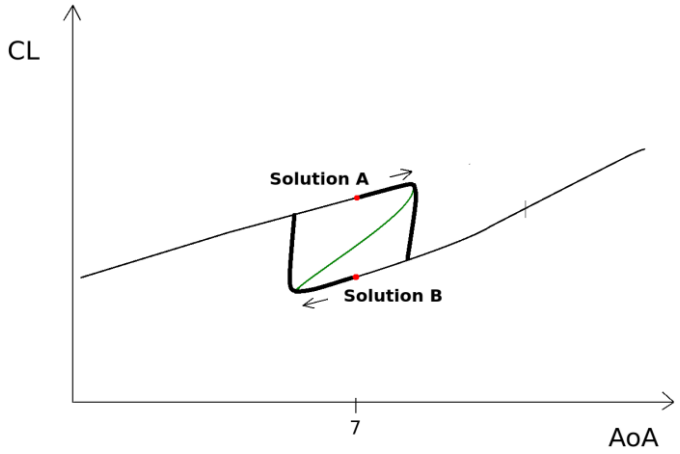

Figure 1.16: Hysteresis loop

This is the fact we want to demonstrate, the existence of an unstable third solution that connects the other ones. To achieve this goal, we are going to use an iterative method by simulating once and again in a similar way as bisection method. We refer to the edge tracking method.

The approach to find the unstable solution is based on bisection method combined, as mentioned before, with numerical simulations. Once we have the two main solutions, we start with the edge tracking method. Its mathematical basis is based on:

$$AB = A - B \tag{1.4}$$

By this way we create a vector which links the two stable solutions. These two velocity fields can be used to reconstruct an initial condition as follows:

$$C_K = B + K \cdot (AB) \tag{1.5}$$

where K ϵ [0,1] is a scale factor. As we have defined it, C(K=1) =A and C(K=0) =B. Therefore, on direction we have created it must be one intermediate value K where an unstable solution does not end in A or B, at least enough time to consider it solution. The approach to finding C is to successively bisect the AB interval as shown in Figure 1.17. To can proceed this method in Nektar++ it is necessary to use the tool *FieldConvert* with its modules Add and Scale. That is for can create C_K, a sum of velocity and pression fields from A and B scaled by K factor.

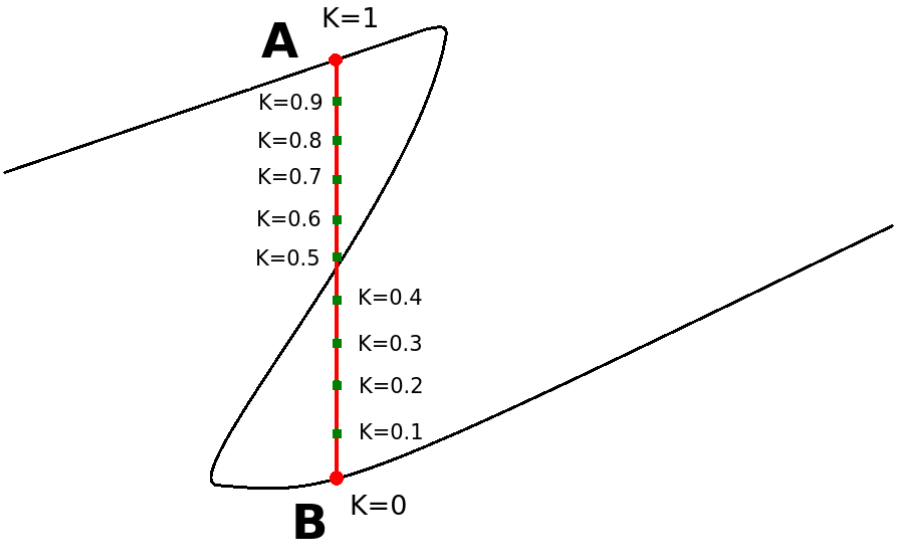

Figure 1.17: Edge tracking method

It is suggested the connection between A and B. By edge tracking method we want to try to move across this frontier as long as possible in order to characterize the unstable solution [5]. To achieve that we need to be so accurate to ensure the maximum time on C.

1.6. Boundary layer detachment

When a fluid moves past an object, in our case an airfoil, the fluid molecules near to it reduces its velocity because of the fluid viscosity. The molecules just above the surface are slowed down in their collisions with the molecules that are in contact with the surface. The farther ones are not affected in the same way. This creates a thin layer of fluid near the surface in which the velocity changes from zero at the surface to the free stream value away from the surface. This is called the boundary layer as shown in Figure 1.18.

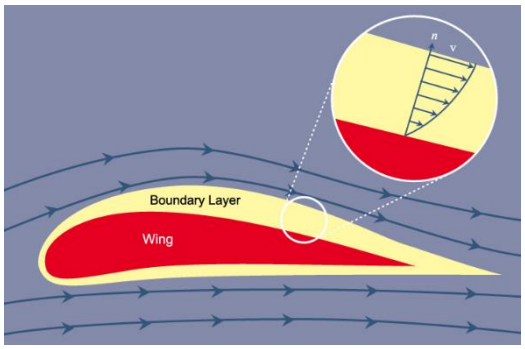

Figure 1.18: Boundary layer near an airfoil

The boundary layer may separate from the body and create an effective shape much different from the physical shape. Flow separation occurs when an adverse pressure gradient occurs in the direction of flow making the velocity at the wall being zero or negative. By increasing the fluid pressure is same to increasing the potential energy of the fluid, leading to a reduced kinetic energy and a deceleration of the fluid. This detachment could lead to a recirculating flux on separation zones and a turbulent wake [6]. In terms of drag, an increase of it.

1.7. Vortex shedding

Von Kármán vortex shedding is called to the periodic detachment of pairs of alternate vortices from a body immersed in a fluid flow, generating an oscillating wake behind it and causing fluctuating forces. This is a situation where the energy subtracted from the flow field by the body drag is not dissipated directly into an irregular motion in the wake, but it is first transferred to a very regular vortex motion. Hence, there is a vorticity printed to the velocity field in the wake. The vortices at either side of the body have opposite directions of rotation, so negative and positive vorticity. These vortices do not mix with the outer flow and are dissipated by viscosity only after a long time [7]. There is a connection with the form drag because of the formation of the vortex shedding.

CHAPTER 2. SIMULATION RESULTS

2.1. Mesh resolution study

Recalling for the main method of this project, one and another simulation must be set up. Therefore, the variable time cannot be forgotten. We realize that simulations expend too much time. In order to reduce this volume of time the software needs to simulate, we thought that an interesting way it was to modify the mesh. The goal was to reduce time, so if we make the mesh be less accurate it will need less time Nektar++. First attempts were focused on reducing the resolution of the mesh but without forgetting in the error we will be making in future simulations with this modified mesh.

Therefore, we try to quantify the error we are making by comparing the results on different simulations. Our reference simulation it will be a full resolution mesh simulation with AoA 9º that will be compared to the other ones at same angle of attack. Modifying the file where the geometry is contained we will be able to apply less resolution on mesh.

The first modification done is in the airfoil parameters from this geometry file, where the mesh and geometry is created. The numbers of points along the airfoil has been reduced all, but in a proper way in order to lose proportional resolution in all directions. This final reduction corresponds to approximately to a 40% in this number of points.

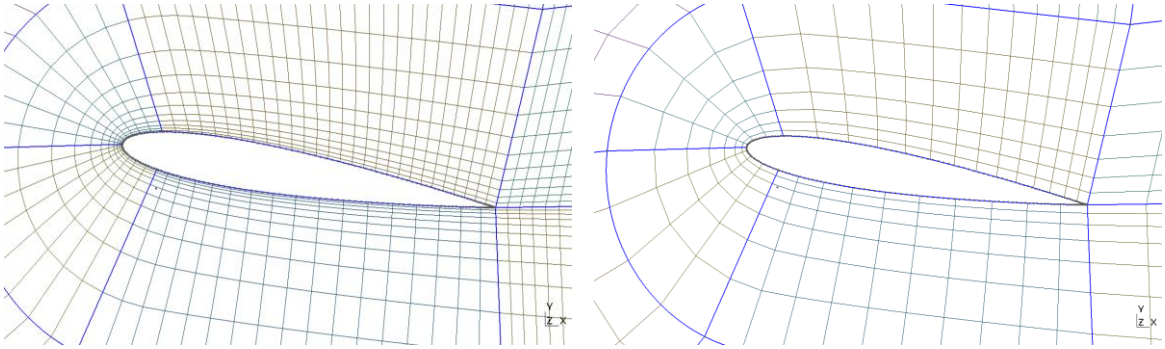

(a) Full resolution mesh (b) Less resolution mesh

Figure 2.1: Comparison of mesh resolution

As can be observed in Figure 2.1, the number of cells have been reduced and making higher the surface per cell. Modifications on geometry file continue for all the lines conforming the mesh. Changing the number of points, it is not the only alteration done. The progression of some points over a line also is a parameter that has helped us to modify the mesh. Remembering that the mesh is a structured one, the Transfinite algorithm gets some weight. It has been so useful to modify directly on the lines were Transfinite was applied, making changes

directly on points that splitted lines and progression of these points. We realize there are surfaces where we can sacrifice more resolution and not be equitable. For example, it is more important the wake than the far field where higher reductions can be assumed.

To achieve the properly modifications, it has been needed to make little changes blindly and quantify the error. If we consider we could adjust a little more we try another time. Notice that for quantify the error is needed to simulate with the selected mesh and compare results with our reference.

In order to quantify error, we choose to compare the aerodynamic forces magnitudes, shown in Figure 2.2. Since the fluid is in motion, we can define a flow direction along the motion. Then, the component of the net force normal to the flow direction is called the Lift; the component of the net force along the flow direction is called the Drag. Lift and Drag are the magnitudes we will compare to quantify the error.

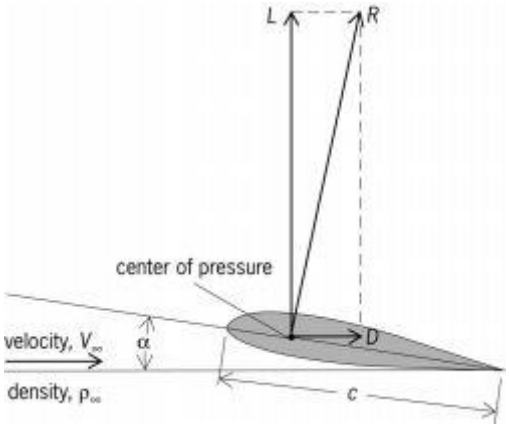

Figure 2.2: Aerodynamic forces over an airfoil.

Next step is to impose the maximum error we want to commit. We set up this value in a maximum of a 0.5% error in comparison with reference forces:

$$e_r = \frac{|F_o - F_r|}{F_o} \cdot 100 < 0.5\% \qquad \textbf{(2.1)}$$

With the help of the software Octave, it is possible to compute the error. When plotting the forces over time, we realize that a periodic behaviour is present.

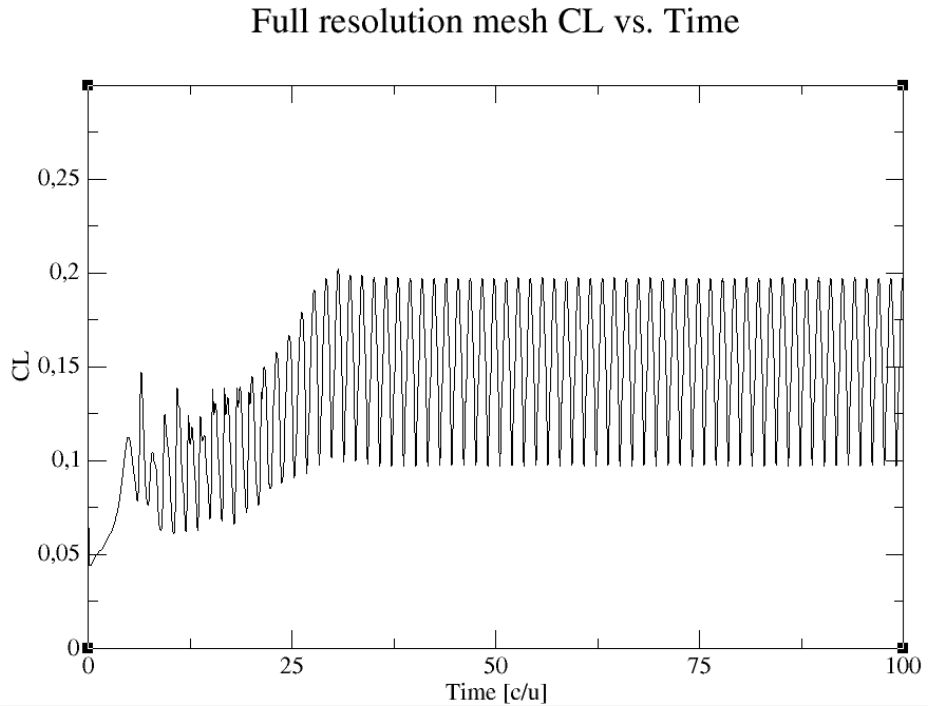

Figure 2.3: Lift over time for full mesh.

In Figure 2.3 there is a first transient mode that disappears to achieve a permanent periodic response. In order to can compare the periodic responses to compute the error, we are going to calculate the mean value of the periodic part. Trying to be as accurate as possible, the intervals for mean value computation will coincide with maximums of the sinusoidal. Thus, we get an entire number of cycles.

	First attempt	Second attempt	Third attempt	Fourth attempt	Fifth attempt	Sixth attempt
Number of points around airfoil reduction (%)	30	36	49	39	55	44
X direction reduction on wake (%)	30	38	60	48	65	55
Y direction reduction on wake (%)	25	35	51	39	58	45
Lift relative error (%)	0.05761	0.1184	4.211	0.2184	15.72	**0.3275**
Drag relative error (%)	0.03656	0.09423	5.079	0.1575	17.39	**0.2759**

Table 2.1: Mesh modifications and relative errors on different simulations

On Table 2.1 is shown the modifications done in the mesh and the relative error obtained in the aerodynamical forces coefficients. The reductions we refer on the table are in respect of the full mesh. We have divided this modifications in the number of points along the airfoils, that they have been described yet few lines above, the reduction on *x* direction and *y* direction. When we do a modification in the number of points along the airfoil we are making changes in both axis, that is why we have separated it. By other way, the other modifications in *x* and *y* are referred the direction where the transfinite algorithm was applied. For example, from the trailing edge until the outlet, it is possible to change the number of points that split the horizontal lines. However, the *y* direction modification impacts also on the *x* direction because of the part that is formed by the curve. The reductions showed on Table 2.1 are a mean value of the modifications done in different parts of the mesh.

Several attempts have been needed to achieve the final modified mesh. Notice the difficulty when trying to increase the error, it has been modified as in an exponential way. That is why we stopped at the last attempt and decide to continue with these results. There is only a 0.05% of difference between axes, so homogeneity can be considered.

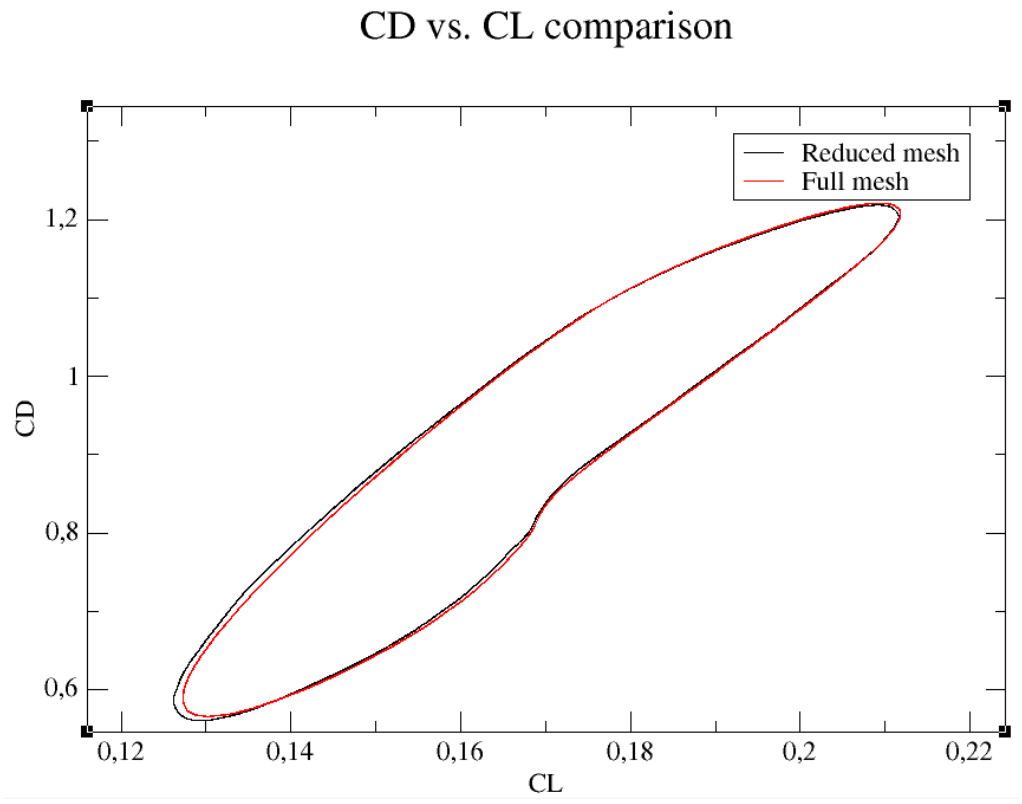

Figure 2.4: Lift comparison between full resolution mesh and reduced mesh.

On Figure 2.4, the adimensionalised forces for the reference mesh and our modified one are compared once arrived to converged solution. As it can be

checked, both solutions are converged and the error is determined by our computation of 0.3275% and 0.2759% for lift and drag, respectively.

A frequency assessment is made also to compute the error we made with this mesh modifications. To can compute this we make the Fourier transform of an aerodynamic force and compare the frequency difference of the firsts harmonic.

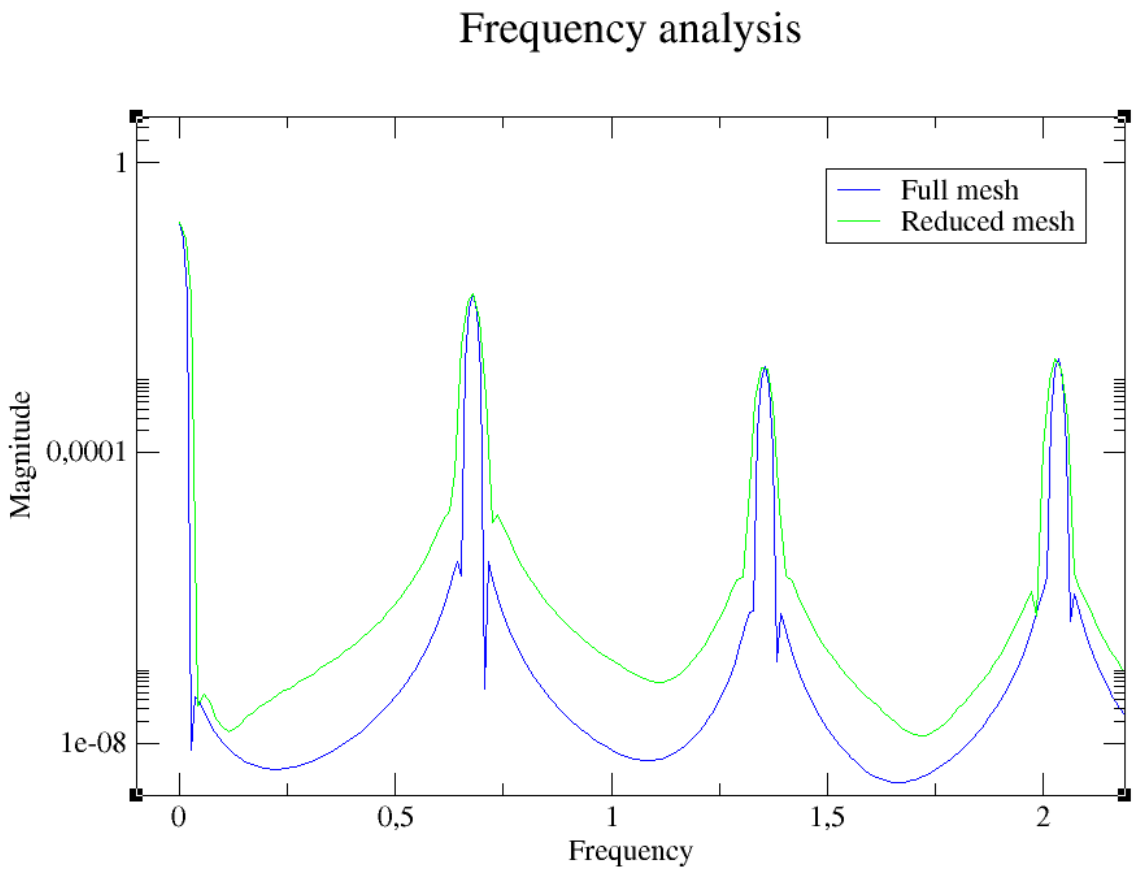

Figure 2.5: Frequency analysis comparison between full mesh and reduced mesh.

In Figure 2.5, we show a few harmonics of the different meshes. We obtain a frequency on the first harmonic of 0.6781 for full mesh and 0.6809 for reduced mesh. This is a 0.41% relative error. There is only a little difference on the peaks of the harmonic but too small. The main difference to consider is located between the peaks, at the valleys. That is because the reduced mesh solution takes more time to arrive to a converged solution and therefore the part we considered to apply the Fourier transform is shorter than in the full mesh, which also has lasted 30 time units longer. Therefore, we can consider errors in the main frequency acceptable. The frequency analysis will be useful on next sections when describing the vortex shedding.

The goal of reducing resolution was the decrease of time simulating. The reduction has been notorious as it is shown in Table 2.2. To compare times, we have decided to display by the console the time needed for 5000 steps.

	Time average [s]
Full resolution	3800
Reduced resolution	840

Table 2.2: Time comparison of different meshes.

2.2. Solutions analysis

First thing to do, is describing the two solution that coexists for AoA 7º. As mentioned before, the parameters we are going to use to describe the solutions will be the aerodynamical forces, lift and drag. These forces can be adimensionalised into their coefficients by the following:

$$C_L = \frac{2L}{\rho V^2 c} \quad \textbf{(2.2)}$$

$$C_D = \frac{2D}{\rho V^2 c} \quad \textbf{(2.3)}$$

But all the variables on the denominator we have defined them as unitary parameters of the simulation, hence:

$$C_L = 2L \quad \textbf{(2.4)}$$

$$C_D = 2D \quad \textbf{(2.5)}$$

This is the relation between coefficients and their respective force. As we always will be in same scenario of parameters on the simulation, we have decided to work with these adimensionalised coefficients.

Time units are dynamic time units because of using unitary chord and velocity. We are not working with seconds.

$$time = \left[\frac{c}{u}\right] \quad \textbf{(2.6)}$$

2.2.1. Solution A

This solution we called A, is achieved with initial conditions starting from rest. Other way, just starting a simulation with no previous flux. It is possible to start directly at our desired AoA or modifying while there is fluid among the airfoil, it will arrive both to same solution.

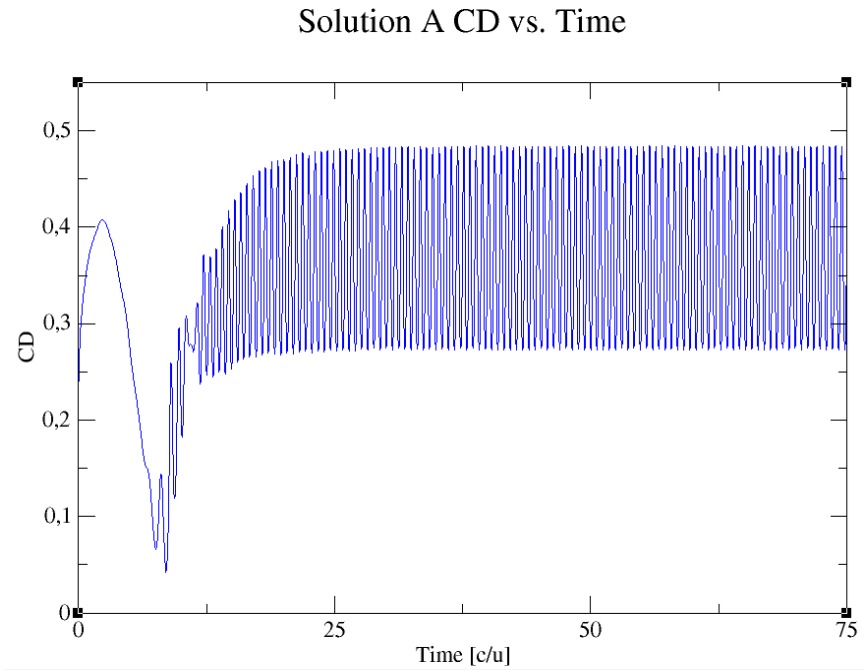

Figure 2.6: CD vs. Time on solution A

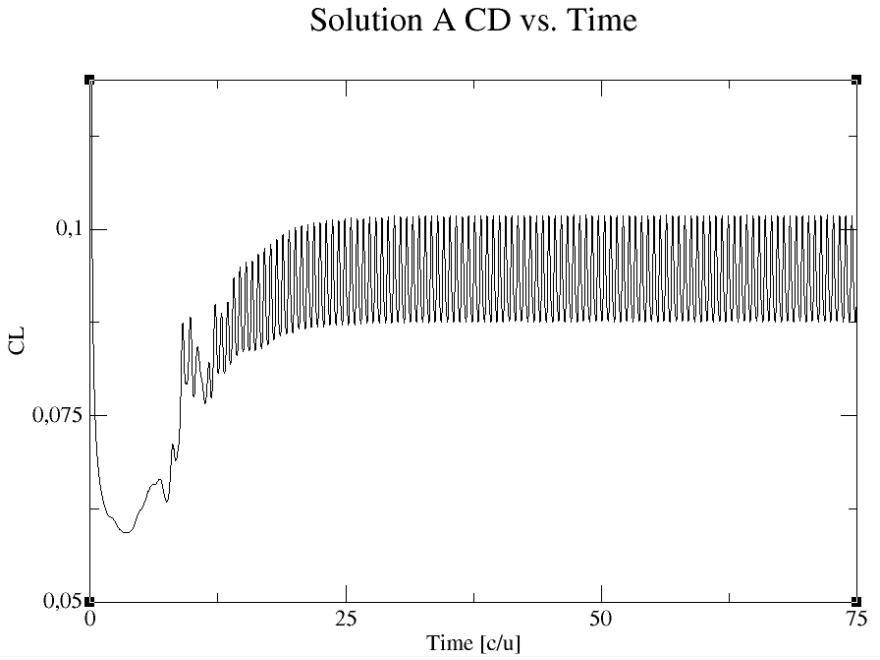

Figure 2.7: CL vs. Time on solution A.

In Figure 2.6 is represented the drag coefficient evolution over time. In a similar way as occurred when comparing aerodynamic forces for AoA 9º, there is a transient mode that govern first moments leading too to a permanent periodic one. Lift behaviour is similar in shape, but reduced in value as shown in Figure

2.7. The maximums achieved by one and another has differences of five times lower for the lift compared to drag.

	Mean value	Amplitude
CL	0.09468	0.007182
CD	0.3798	0.106

Table 2.3: Aerodynamic forces of solution A.

2.2.2. Solution B

By other hand, there is the other solution obtained by coming from the contrary way. That is from not null initial conditions and reducing AoA from 8º to 7º. Therefore, there is an existent flux over the airfoil, a permanent velocity and pression field is achieved and from that point we are going to change angle of attack in order to can arrive solution B.

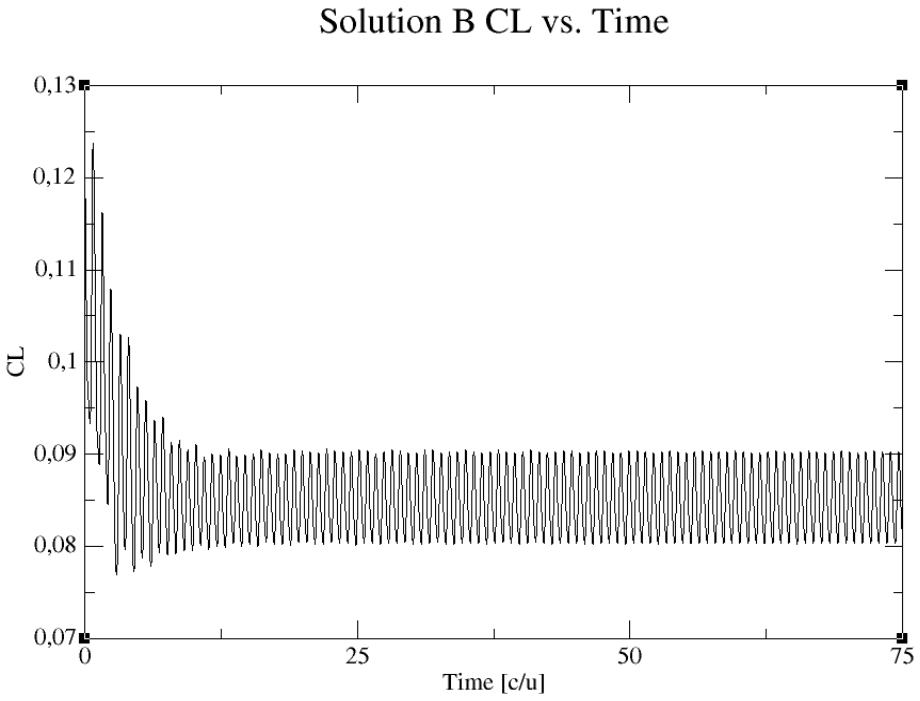

Figure 2.8: Lift vs. Time on solution B.

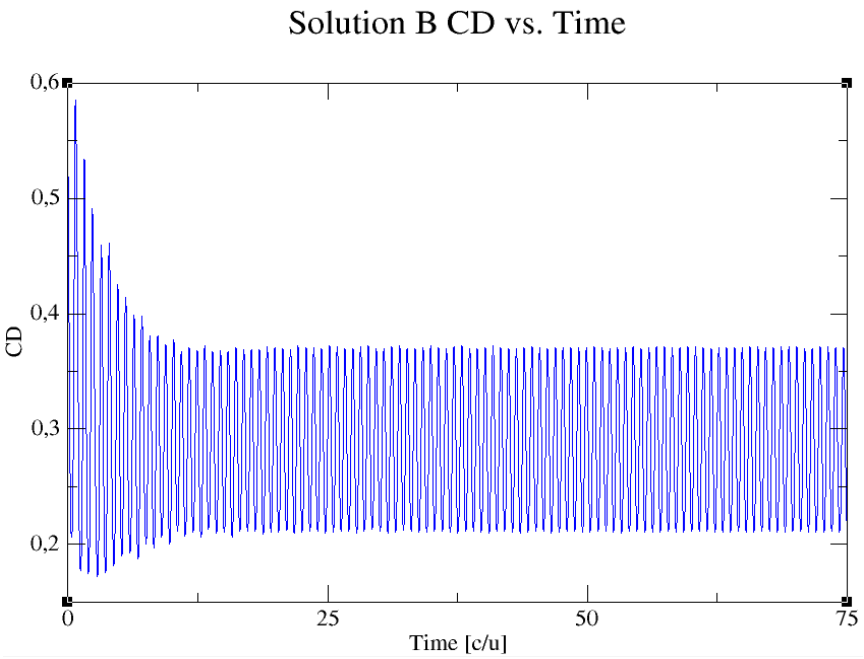

Figure 2.9: Drag vs time on solution B.

Both forces, as we expected, are different from the other solution. Lift and drag responses, shown in Figure 2.8 and 2.9 respectively, are another time, when transient disappears, permanent periodic solutions. First thing we notice is the change done in transient mode. On solution B, there is not a steady interval at the beginning so from initial time exists lift and drag. For that reason, less time in needed to enter in permanent mode.

	Mean value	Amplitude
CL	0.08532	0.005061
CD	0.2914	0.08402

Table 2.4: Aerodynamic forces of solution B.

2.2.3. Comparison

Comparing both solutions, there is a little decrease in solution B for lift and drag. Lift reduced its mean value in solution B in approximately a 10%, while drag has a higher reduction nearly the 20%. Amplitudes of both sinusoidal has also achieved lower values, nearby 30% and 20% for lift and drag, respectively. In Figure 2.10 is shown in an easily way this variance between aerodynamic forces for both solutions, in addition with results for AoA 8º and 9º to get a better comparison.

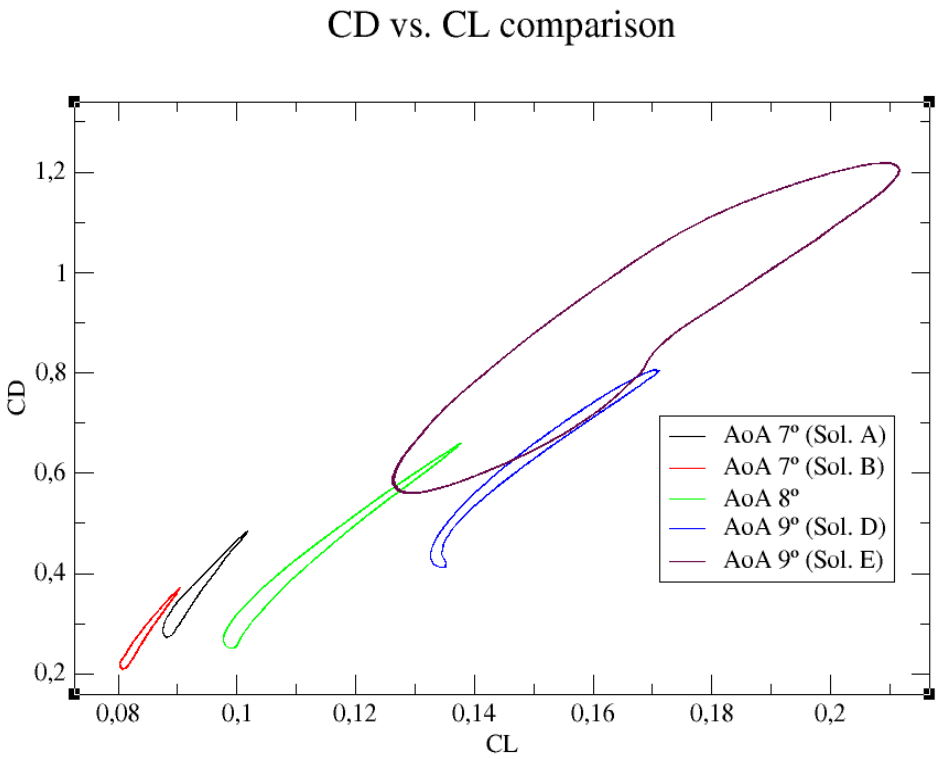

Figure 2.10: CD vs. CL of different solutions.

In order to have more comparative solutions, we recall for AoA 8º and 9º simulation. This will help us to introduce some characteristics as the boundary layer detachment or the vortex shedding. First to remark is the huge difference between solution for AoA 7º and for AoA 9º. Also, recalling the Figure 1.15 and with help of Figure 2.10, we can check that there is an evolution of solutions. There is a smooth evolution from Solution B to AoA 8º. Notice that for AoA 9º we have plotted also two solutions. We had suspicions that for this value of angle of attack it exists another case of hysteresis. We can check that solution D is the continuation of the evolution from AoA 8º. Then, same as occurs at AoA 7º a double saddle node lets up to solution E. Solution E is the most different from other solutions, and show us that is a different hysteresis case from the which one we are studying.

As we expected, aerodynamic forces have been increased with the increase of the angle of attack. On Table 2.5 and 2.6 there are the values of AoA 8º and 9º, respectively, that describes the sinusoidal permanent state and the multiplying factor they have increased in respect with AoA 7º solution B.

	Mean value	Increase factor	Amplitude	Increase factor
CL	0.1178	1.38	0.02008	3.97
CD	0.4558	1.56	0.2047	2.44

Table 2.5: Aerodynamic forces of solution at AoA 8º.

	Mean value	Increase factor	Amplitude	Increase factor
CL	0.1519	1.78	0.01934	3.82
CD	0.6099	2.09	0.1984	2.36

Table 2.6: Aerodynamic forces of solution at AoA 9º (Sol. D).

There is a remarkable increase in all values, but the higher ones occurred in terms of amplitude. Lift increase get linked with the increase of angle of attack but its evolution is smooth, same as occurred with the drag that gets a few higher increase factors while increasing the angle of attack. Concerning the drag, we have two types, the friction and pressure/form drag. The friction drag is caused by the friction of a fluid against the surface of an object that is moving through it. There is also the form drag that is caused by the separation of the boundary layer from a surface and the wake created by that separation. As we will see later when talking about boundary layer detachment and vortex shedding, this type of drag gets the higher relevance of drag increase mentioned.

2.2.4. Boundary layer detachment

We need to include in the study the boundary layer detachment. We are going to compare the different solutions and the detachment that occurred. To can visualize this phenomenon we are going to compute the streamlines near the airfoil and can determine where this boundary layer detachment occurs.

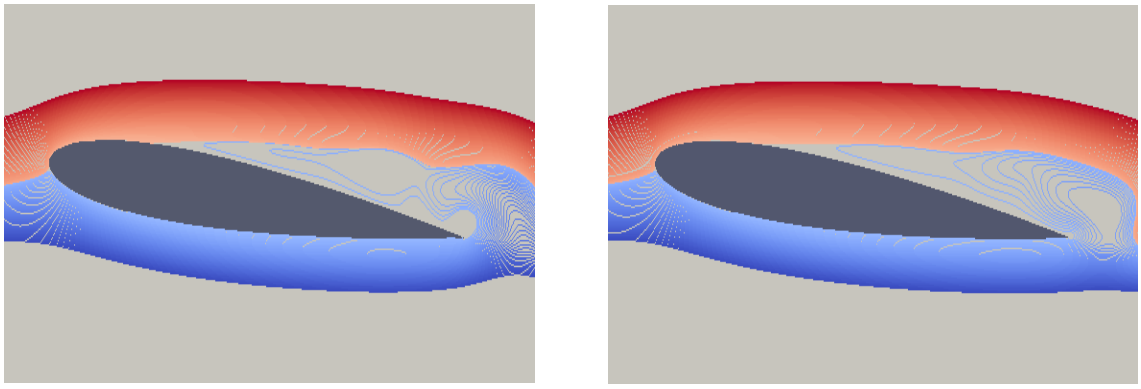

(a) Solution A (b) Solution B

Figure 2.11: Streamlines for AoA 7º solutions.

On Figure 2.11 are shown for both solutions the streamlines near the airfoil. The detachment is produced when the nearest red streamline is separated from the airfoil. As it can be checked, it occurs at the same distance in both solutions. Perhaps the recirculating bubble performed when boundary layer detachment occurred presents some differences.

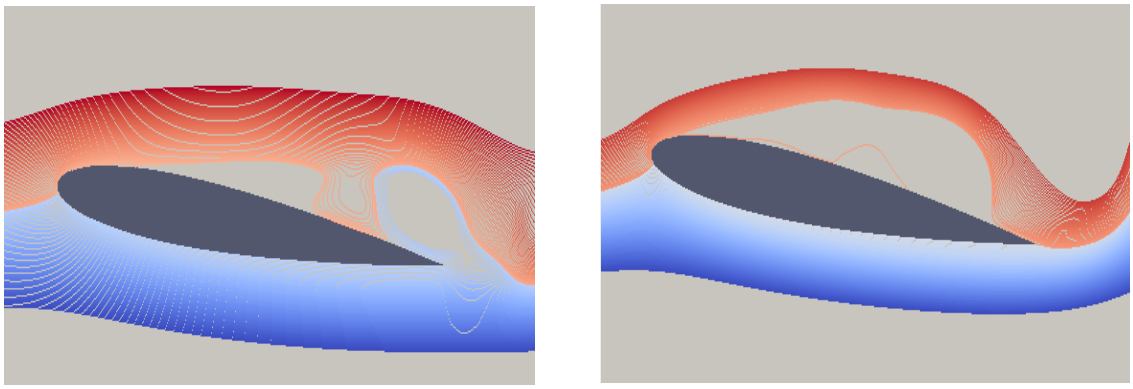

(a) AoA 8º (b) AoA 9º (Sol. E)

Figure 2.12: Streamlines for AoA 8º and 9º (Sol. E)

In Figure 2.12 we show the streamlines for the solution at AoA 8º and 9º case E, and as expected the detachment occurs nearer the leading edge than in AoA 7º as the angle of attack increase. In solution A, the detachment occurs at the mesh geometric location on x axis of -0.75 meanwhile for AoA 8º at -0.79 and for AoA 9º case E it occurs at -0.905. Therefore, there is a relation between de angle of attack and the boundary layer detachment. The higher angle of attack the earlier occurs the detachment.

2.2.5. Vortex shedding

With the software Paraview we have all the tools to compute vorticity and visualize the vortex shedding. This phenomenon, as commented in section 1.7, increase the form drag.

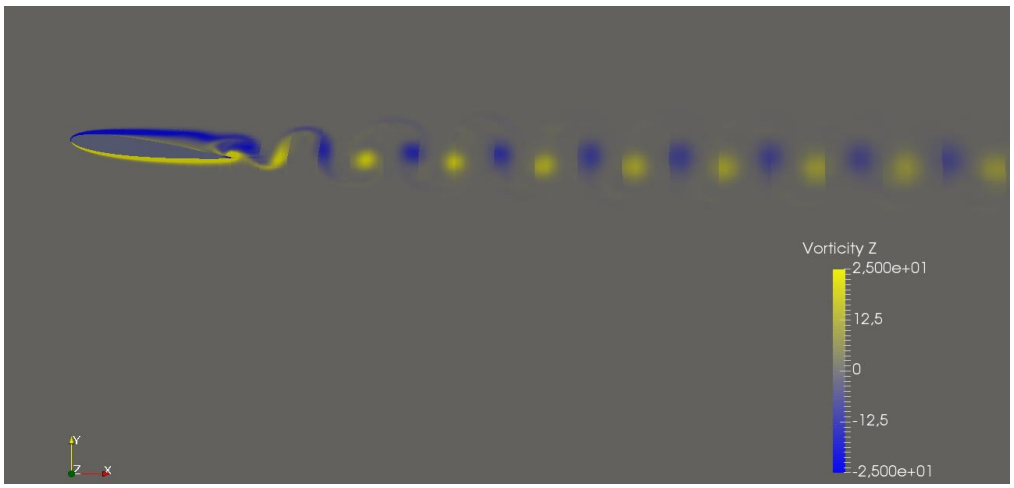

Figure 2.13: Vortex shedding for solution A.

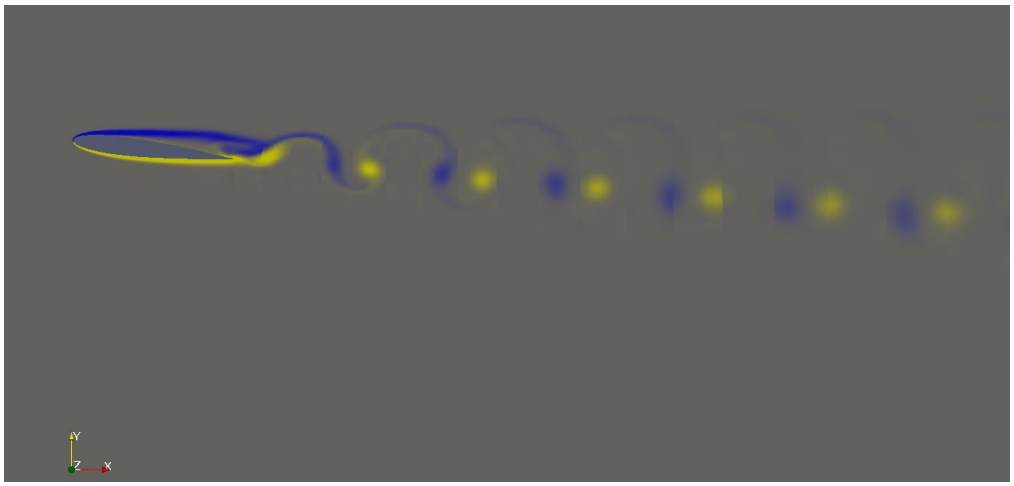

Figure 2.14: Vortex shedding for solution B.

Vorticity calculation has been need to can show the vortex shedding. These results on the vortex shedding ensure that they are different solutions one from another. First thing to remark, is the difference on the period these vortices detach. On solution A, the period is lower so the frequency is higher than in solution B. On case B, both vortices are closer one to another but the time for start another cycle is higher. The vortices are more clearly paired, while solution A features a train of braided vortices. There is also a difference on the direction these vortices are oriented, called the vortex street. In solution A follows a normal trajectory along horizontal axis, clearly aligned with free stream velocity, but in case B this direction is a little pushed downwards. Figure 2.13 and 2.14 shows all of these details. They are showed one above the other to do not lose resolution when compressing the images. The higher vortices creation in solution A gets linked with the higher drag force experimented in that case, where solution B produces less vortices therefore drag is lower for these low Reynolds number as showed in Table 2.7.

	Solution A	Solution B
CD	0.3798	0.2914

Table 2.7: Drag coefficient for solutions A and B.

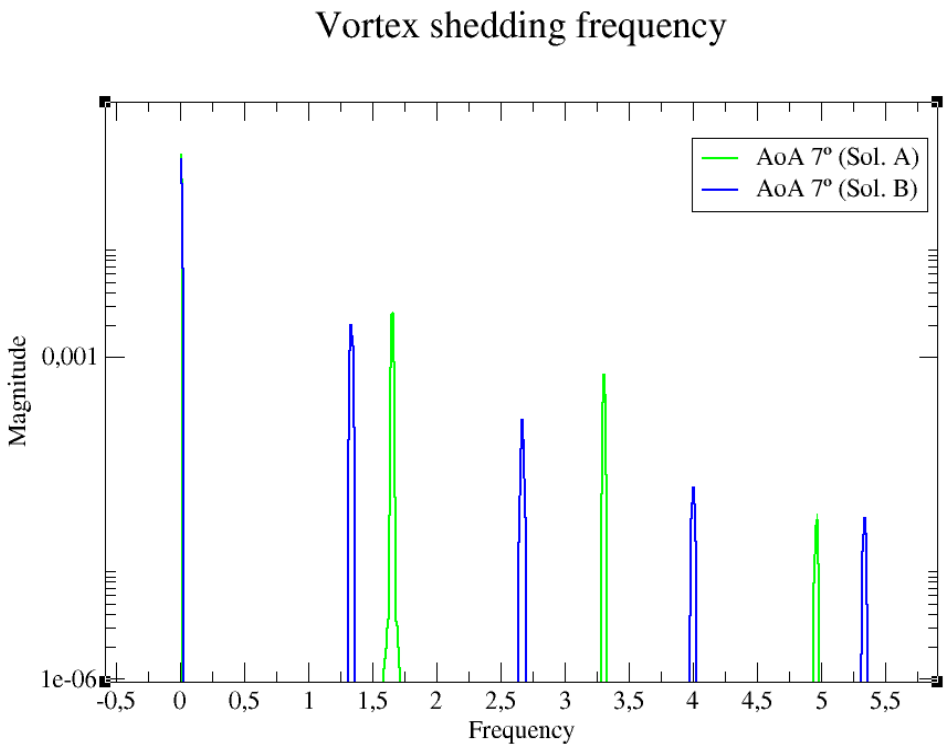

Figure 2.15: Vortex shedding frequency for solutions A and B.

With the frequency analysis of Figure 2.15, we can quantify the difference on the frequency of the vortex. As checked in the figures obtained with Paraview, we have a higher frequency on solution A which is centred in a frequency of 1.655 for the first harmonic. By other way, B has less frequency in vortex detachment, 1.337. There is a remarkable difference of 19% due to differences in the aerodynamic forces between both solutions.

As we have done before with lift and drag, including the results of AoA 8º, we are going to make the same with vortex shedding to have a better comparison scenario and a third reference to compare.

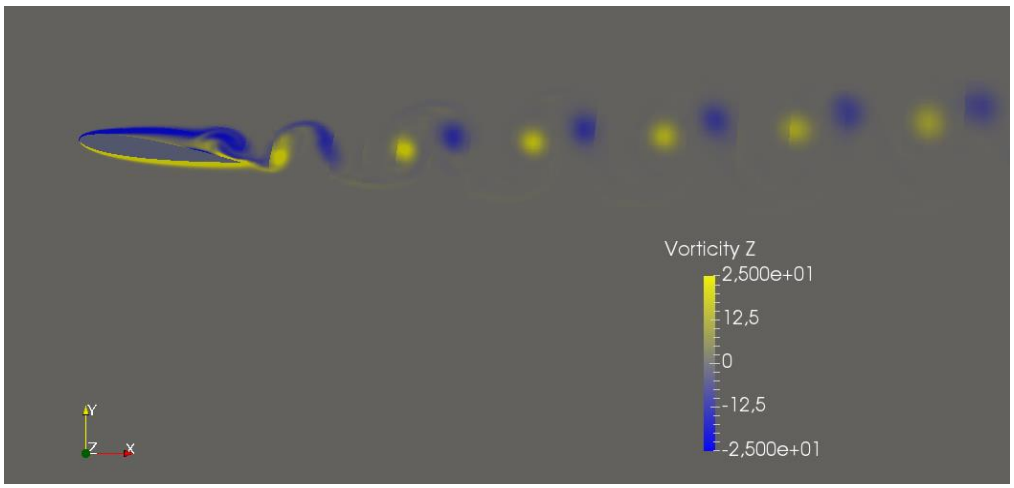

Figure 2.16: Vortex shedding for AoA 8º.

In Figure 2.16 is computed the vorticity to show the vortices for solution at AoA 8º. The main difference we find respect the other cases is the vortex street. In this case the vortices are pushed upwards. It is a closer solution to solution B because the vortices are more clearly paired, meanwhile in solution A it is not.

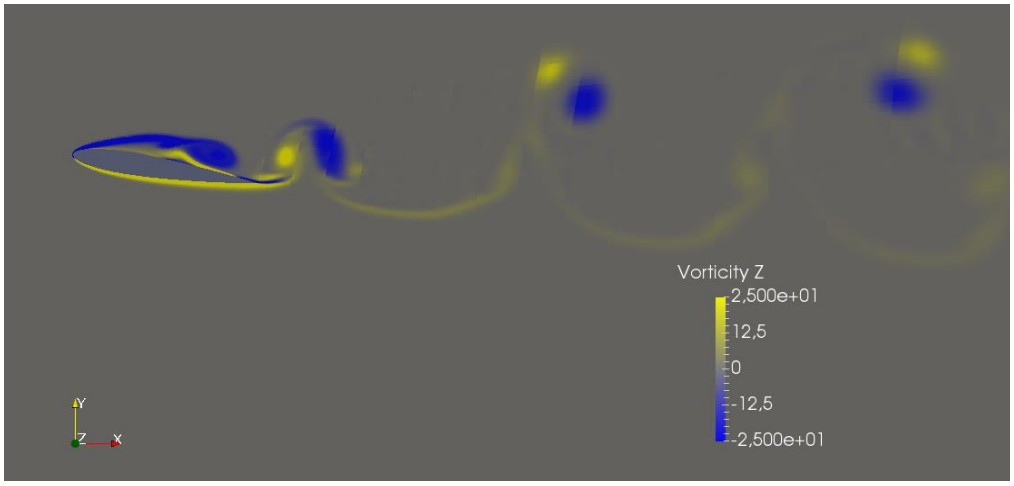

Figure 2.17: Vortex shedding for AoA 9º (Sol. E)

If we take a look to vorticity measurements for AoA 9º in Figure 2.17, we find a very different solution from both before. The hysteresis located at this angle of attack has completely changed the shape of the vortex shedding. We want to show AoA 9º case E because of the notable difference obtained. The vortex frequency has decreased considerably, however the vortex size suffered a notable augmentation. Upper side and downside vortex are closer again. The vortex street has been pushed upwards more abruptly compared with AoA 8º.

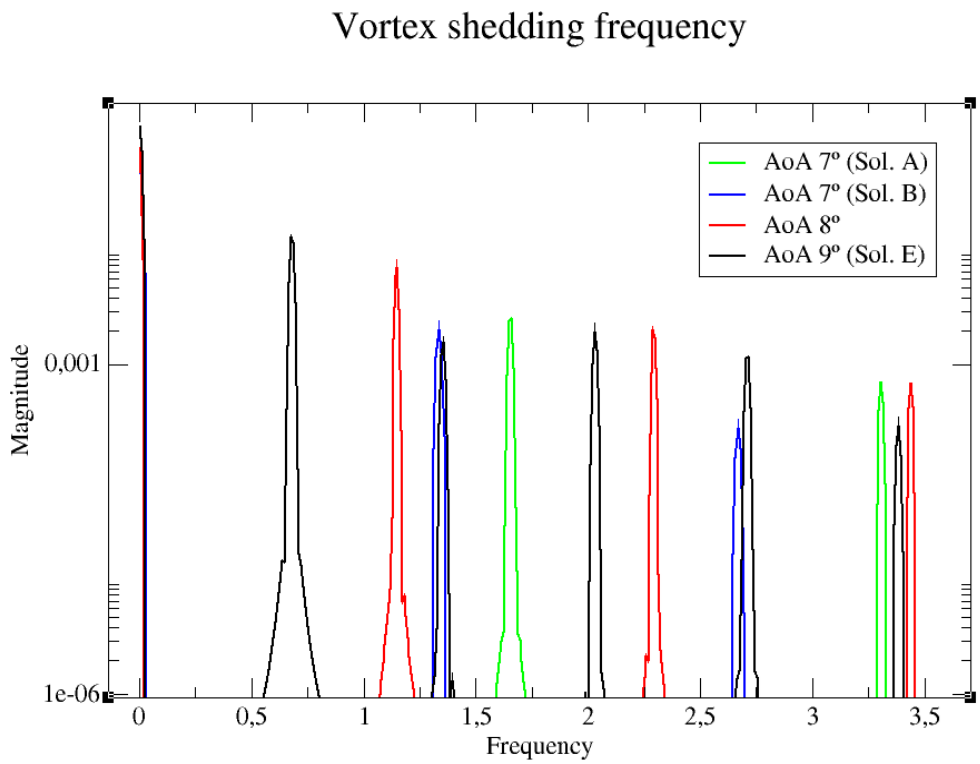

Figure 2.18: Vortex shedding frequencies for the different solutions.

The frequency decrease is showed in Figure 2.18, and also can be appreciated on the image computed with Paraview. The first harmonic for AoA 8º is centred in 1.151 that corresponds to a nearly 30% decrease compared with solution A. For AoA 9º case E the frequency reduction is higher, having the main peak centred at a frequency of 0.6798. This is a reduction of approximately a 60% comparing it with solution A. In both cases also the magnitude of the first harmonic is different, meanwhile A and B where quite similar. We cannot relate this higher magnitude with the size of the vortex, because AoA 8º is 7 times higher the value and yet the size of the vortex is similar to solution A or B.

2.3. Edge tracking analysis

The edge tracking method lead us to define this solution. As showed in Figure 1.16, we start dividing this vector that links A and B and changing values of K in order to determine in which section bifurcation has occurred. The magnitude we have chosen to observe this bifurcation is the lift force but the pressure component. This decision is made for the easy appreciation for the separation of solutions. The pression component of the lift is plotted against dynamic time.

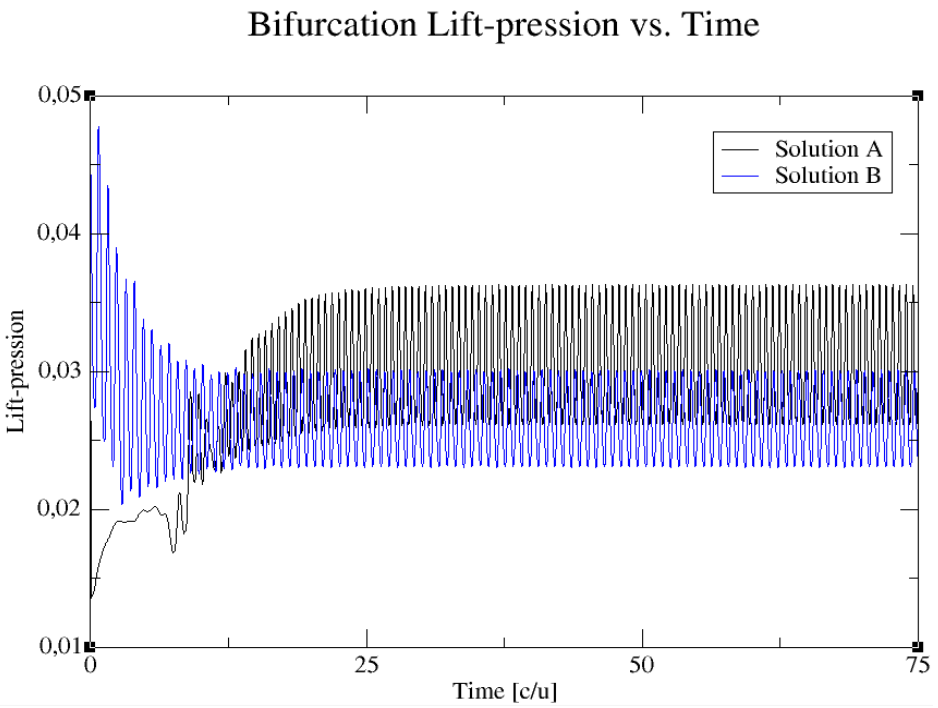

Figure 2.19: Lift pression component vs. Time on solutions A and B.

Comparing both responses on Figure 2.19, it is easy to recognize when we are in one or another solution. If we have a look at the permanent mode, the maximum values of the sinusoidal are the values on which we pay attention. For case A this value is near the 0.036 N and in case B approximately 0.03 N. Then we start the simulations by the edge tracking method. First bifurcation we have found between K values 0.4 and 0.5.

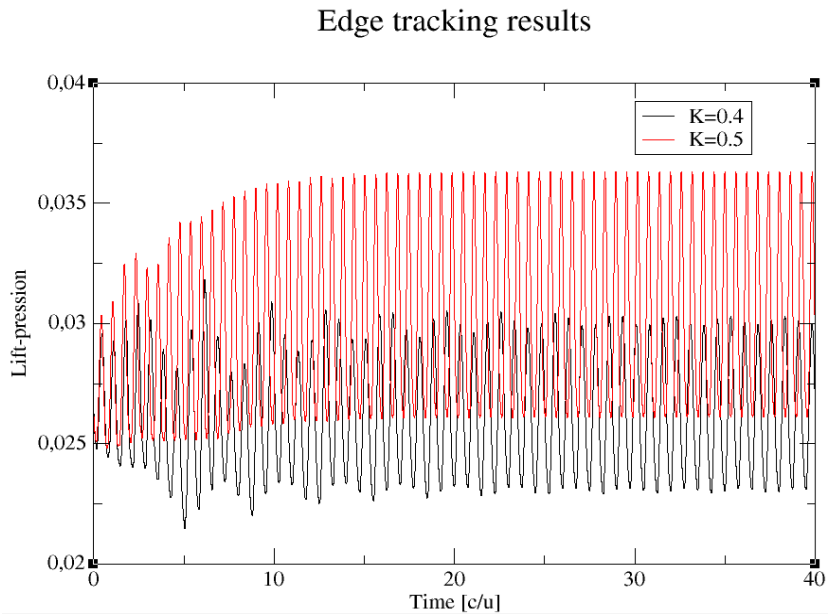

Figure 2.20: Edge tracking results for K=0.4 and 0.5.

In Figure 2.20 it is only possible to distinguish both solutions, but not enough about solution C. Rapidly it tends to A or B. We need to accurate more to get more information about C.

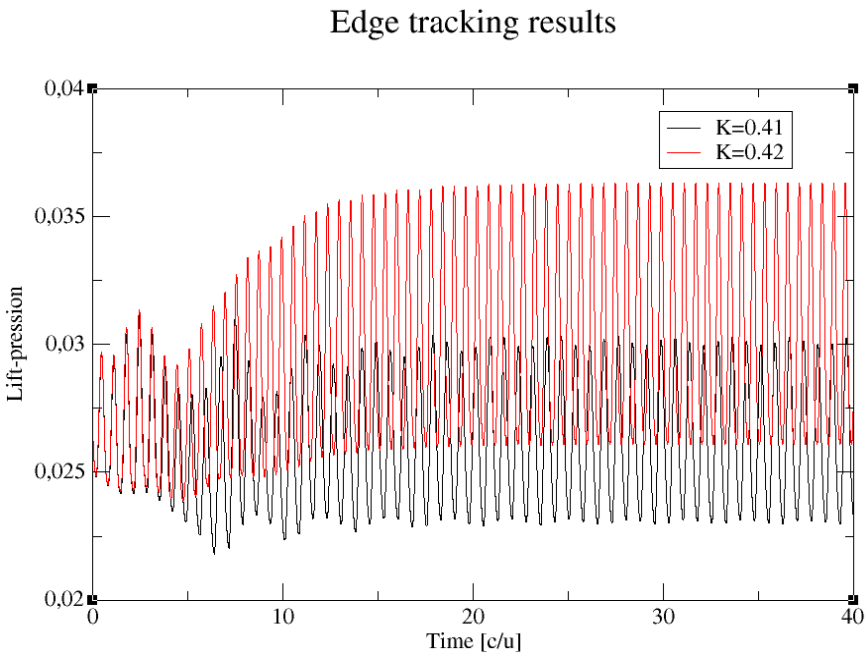

Figure 2.21: Edge tracking results for K=0.41 and 0.42.

With only one more decimal it is possible to start to distinguish the appearance of a new response in Figure 2.21. It still lasts for small time lapse, around 5 seconds, but it is common for the two cases until the bifurcation occurs. We can appreciate that it is also a periodic response.

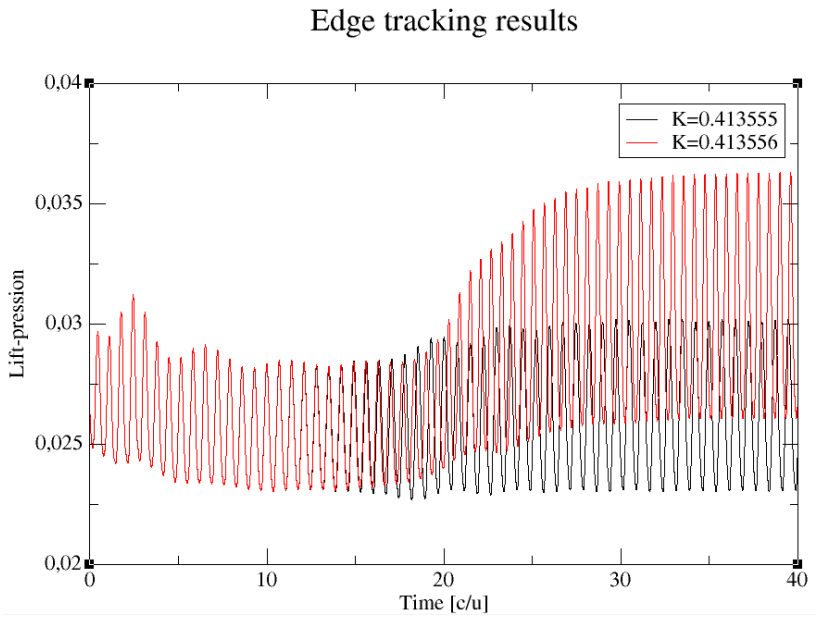

Figure 2.22: Edge tracking results for K=0.413555 and 0.413556.

As we expected, while we are more accurate we can stay more time on solution C. In Figure 2.22 we can describe solution C for approximately 15 seconds and then it tends to one solution or another. However, the periodic oscillation of C starts to get converged. This is a signal that tells us C is a solution, unstable but solution.

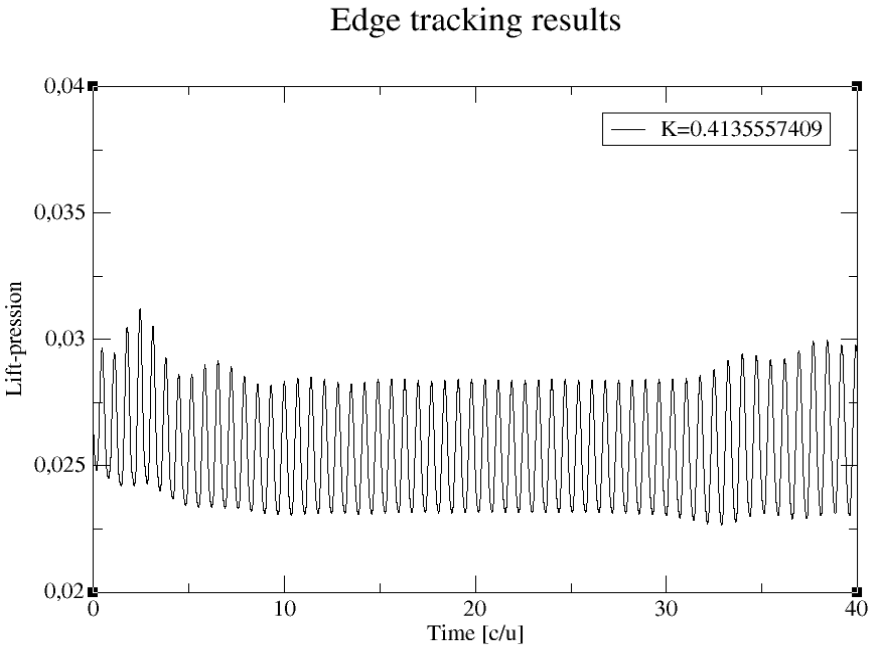

Figure 2.23: Edge tracking results for K=0.4135557409.

On Figure 2.23, we show our last simulation. Due to time limitations, it has not been possible to accurate more on edge tracking. However, we can appreciate a periodical solution of approximately 30 seconds. In Figure 2.24, we show the almost converged solution by plotting the aerodynamic forces between them.

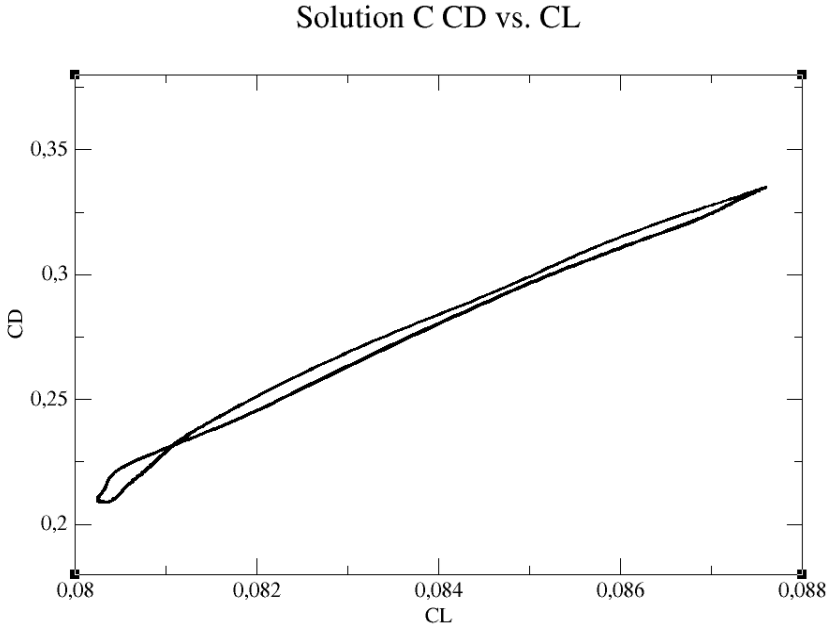

Figure 2.24: CD vs. CL of Solution C.

In order to can characterize this solution, we need to show the aerodynamic forces that describes it to can analyse them and compare with solutions A and B.

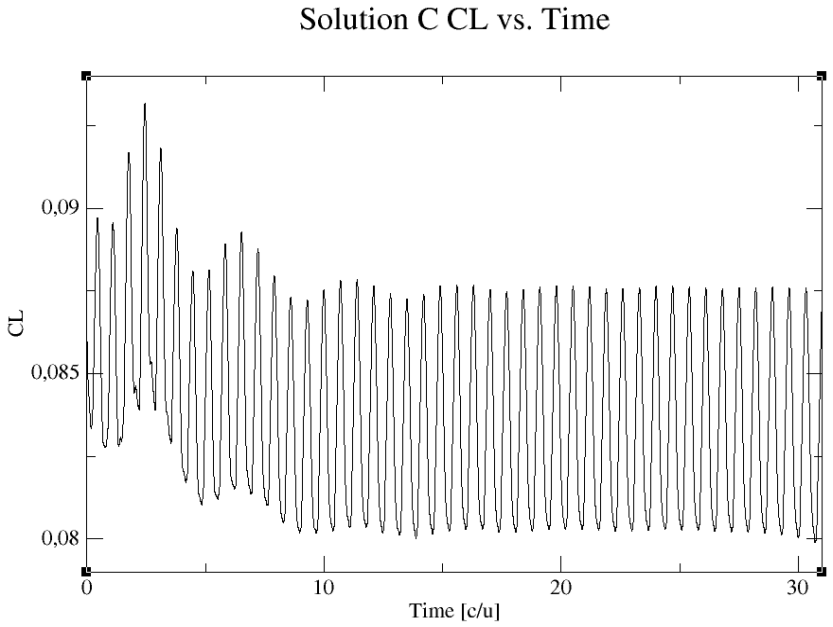

Figure 2.25: CL vs. Time on solution C.

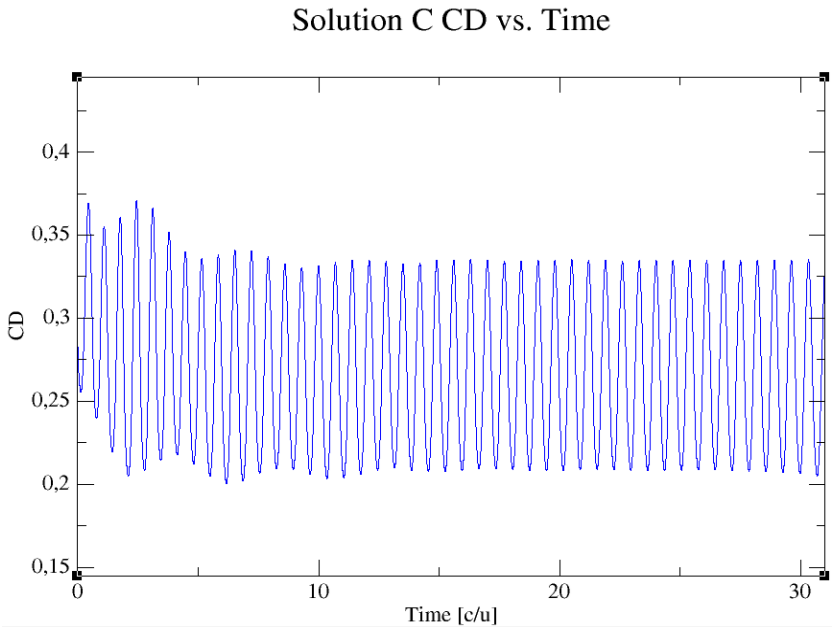

Figure 2.26: CD vs. Time on solution C.

Same as has occurred in the other cases, on Figure 2.25 and 2.26 there is a transient mode that precedes a permanent mode. It is also a periodic solution, for

both aerodynamic forces. It is possible to enlarge the permanent mode being more accurate on the scale factor, but it is a limitation to us as commented before because of time required. On the Table 2.8 we show the characteristics of the permanent response of aerodynamic forces on solution C.

	Mean value	Amplitude
CL	0.08396	0.00367
CD	0.2714	0.0629

Table 2.8: Aerodynamic forces of solution C.

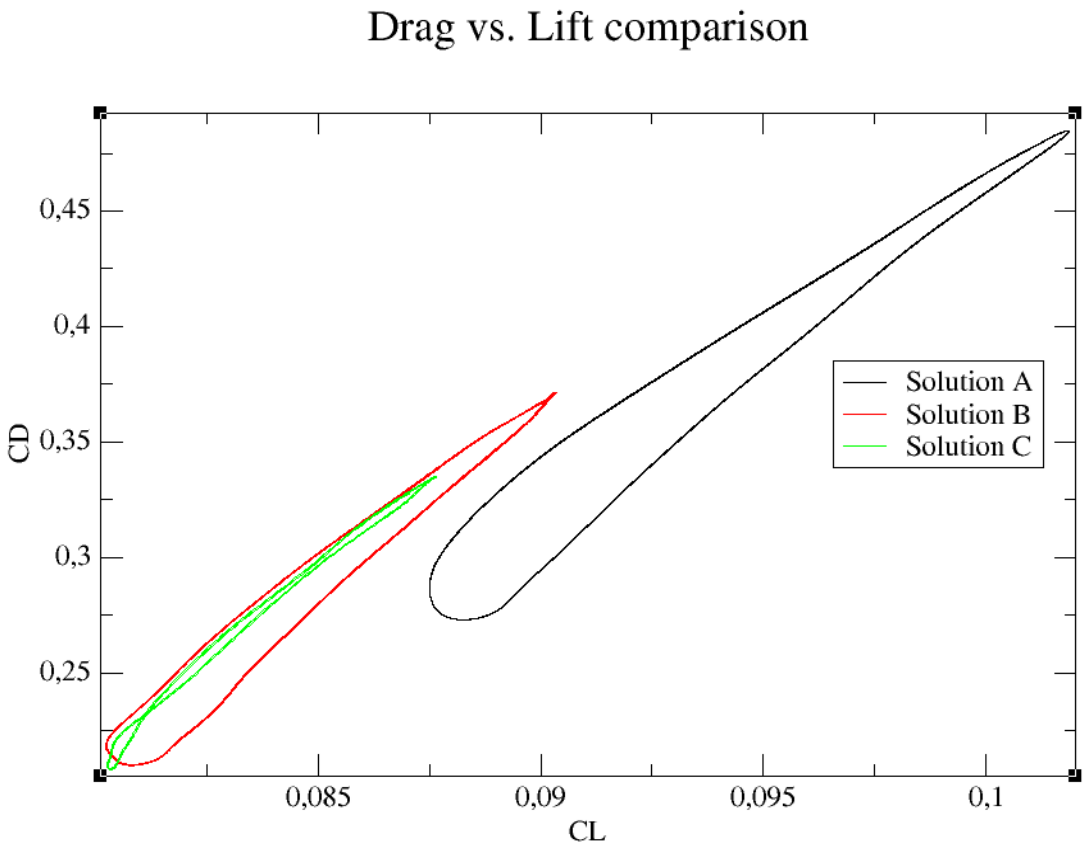

Figure 2.27: CD vs. CL of all solutions at AoA 7º.

On Figure 2.27 it is possible to distinguish the three different solutions that occurs at AoA 7º. All of them are different between them. Solutions A and B are the stable solutions and their shape looks quite similar despite of their values. Solution C, the unstable one, has a different shape. However, the values are more similar to B than to A. On Table 2.9 and 2.10 are showed all the values of the aerodynamic forces for all the solutions obtained at AoA 7º.

Lift coefficients for all solutions at AoA 7º:

Solution	Mean value	Amplitude
A	0.09468	0.007182
B	0.08532	0.005061
C	0.08396	0.00367

Table 2.9: CL values of the different solutions at AoA 7º.

Drag coefficients for all solutions at AoA 7º:

Solution	Mean value	Amplitude
A	0.3798	0.106
B	0.2914	0.08402
C	0.2714	0.0629

Table 2.10: CD values of the different solutions at AoA 7º.

2.3.1. Boundary layer detachment

Same as done before, the streamlines of the fluid will help us to concrete where the boundary layer detachment happens.

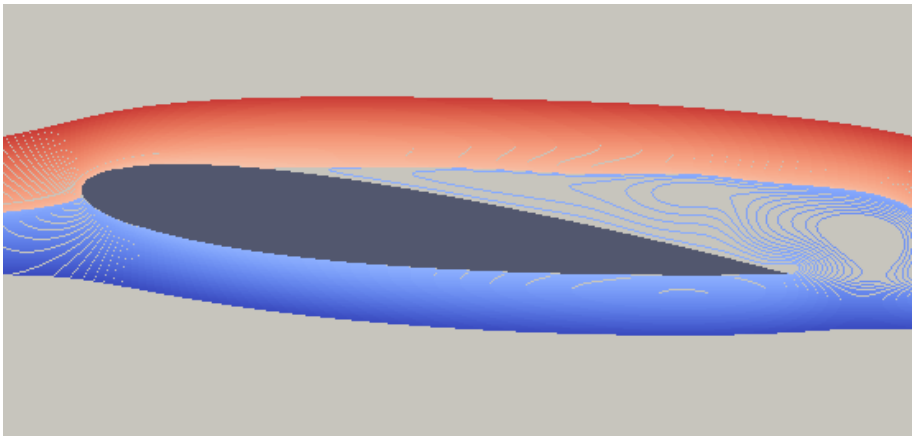

Figure 2.28: Streamlines for solution C

As we expected, we are in a similar case than in solution A and B. As shown in Figure 2.28, the detachment occurs at the same geometric location because of the same angle of attack of these three solutions. The boundary layer detachment

does not bring us more information to describe solution C as it occurs equals than in the other ones.

2.3.2. Vortex shedding

The last case we need to compare is the vortex shedding. We expect something similar to case B because drag values are more common to this solution.

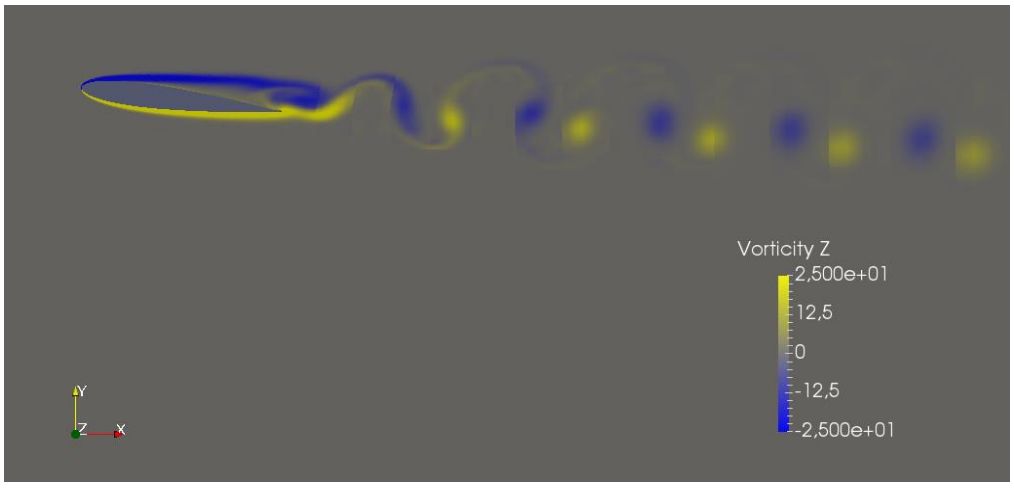

Figure 2.29: Vortex shedding for solution C.

On Figure 2.29 we obtain the vortex shedding for C. It is similar to B but not at all. The frequency of the vortex has increased. Deviation towards down is maintained but not with same inclination, on this case is more near to horizontal. Separation between vortex is a little bit higher.

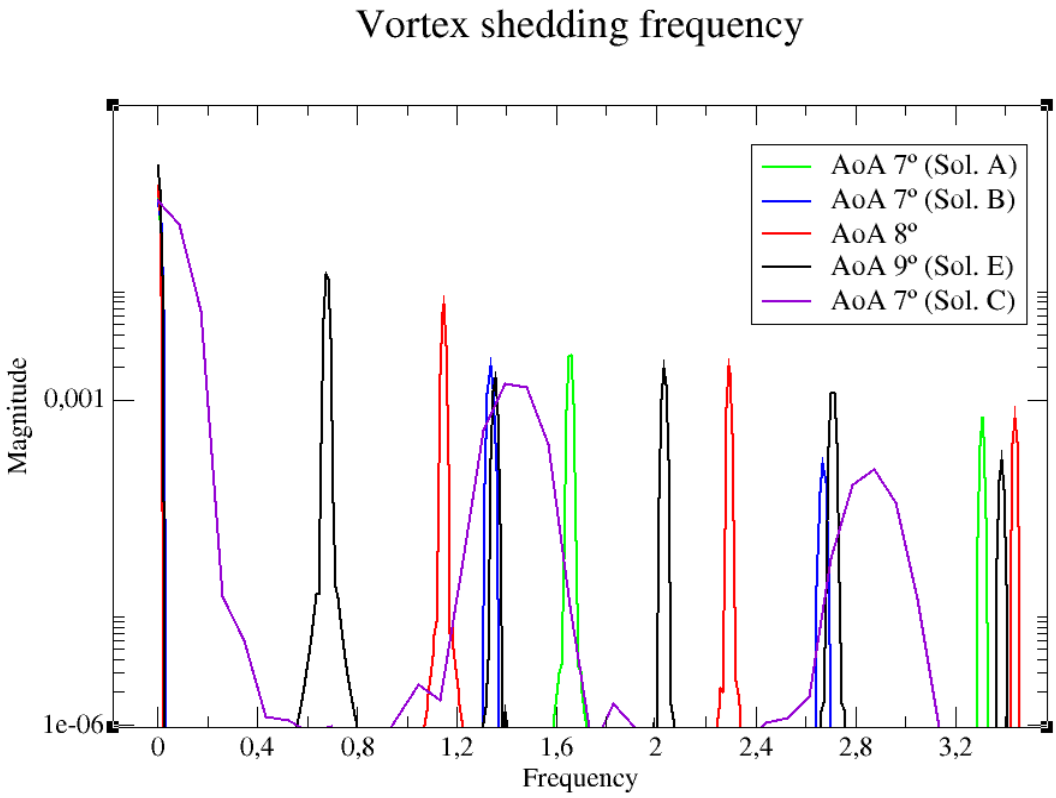

Figure 2.30: Vortex frequency of all solutions.

On Figure 2.30 we have the overview of the frequency analysis of all the solutions. As we can observe qualitatively with Paraview, vortex frequency of C is higher than B but not as big as A. We have a frequency in C of 1.441. We also can see the shape of the harmonic of solution C differs with the rest of the solutions. This is because the accuration of the scale factor. With a few more time we could get some decimals that help to solution converge better.

We can assume that solution C is topologically closer to solution B than to A. In other words, the saddle-node intervening between A and C introduces more noticeable changes than the other one. The vortex pairs are still visible as in case B, but their arrangement in a train as it occurs in A starts to be noticeable.

CONCLUSIONS

The different analysis made and the results obtained, perhaps it is not the best accuration realized, leads us to demonstrate the existence of an unstable solution region. It has been necessary an exhaustive analysis also of the other solutions that coexists to can characterize and differentiate each one.

The edge tracking method leads us to be able to make this affirmation. The lack of time does not let us to be more accurate which by this way we could describe better the solution C.

The vortex shedding has an important relation with the frequency of the aerodynamic forces when arriving a permanent mode and can differ enough with just low changes.

The low-Reynolds studies help us to understand better what happen at higher Reynolds number where mathematical models are needed to describe physics. Low-Reynolds studies can be considered easier but are helpful because the achievements are useful. The different phenomena that governs the high-Reynolds number are more difficult to characterize and sometimes it is impossible and only can be approximated, as in case of high turbulences.

Active flow control may help select one of either solutions when hysteresis exists. It will depend on the aerodynamical performance required for the user to activate one or another solution.

This is a 2D analysis. The hysteresis may disappear with the three-dimension extension study and probably it will introduce more complex phenomena for analysis.

BIBLIOGRAPHY

[1] Yang , Z. , Igarashi, H., Martin, M. and Hu, H. “An experimental investigation On aerodynamic hysteresis of a low-Reynolds number airfoil.” *AAIA Aerospace Sciences Meeting and Exhibit*, 46th (January 7-10, 2008)

[2] Kerswell, R. “Edge tracking – Walking the tightrope”, Lecture 8.

[3] Department of Aeronautics, Imperial College London, UK and Scientific Computing and Imaging Institute, University of Utah, USA. Nektar++: Spectral/hp Element Framework. (Version 4.4.0, March 8, 2017)

[4] C. Geuzaine and J.- F. Remacle, Gmsh: a three-dimensional finite element mesh generator with built-in pre- and post-processing facilities. International Journal for Numerical Methods in Engineering 79(11), pp. 1309-1331, 2009.

[5] J.D. Skufca, J.A. Yorke & B. Eckhardt, “Edge of chaos in a parallel shear flow.” *Phys. Rev. Lett.*, 96, 174101, 2006.

[6] Mueller, T. J., “The influence of laminar separation and transition on low Reynolds number airfoil hysteresis”. *Journal of Aircraft*, Vol. 22, No. 9, 1985 , pp763-770.

[7] Rong F. Huang and Chih L. Lin. "Vortex shedding and shear-layer instability of wing at low-Reynolds numbers", AIAA Journal, Vol. 33, No. 8 (1995), pp. 1398-1403.

[8] White F. M., *Fluid Mechanics,* McGraw-Hill Education; 8th Edition (February 16th, 2015).

[9] Pozrikidis C., *Fluid Dynamics: Theory, Computation and Numerical Simulation* Springer; 2nd Edition, ed. 2009 (June 10th, 2009).